AD-A097 448 SANDIA NATIONAL LABS ALBUQUERQUE NM F/G 14/5
PHOTOFERROELECTRIC IMAGE STORAGE IN PLZT CERAMICS.(U)
MAR 81 C E LAND, P S PEERCY AT(29-1)-789
UNCLASSIFIED ARO-15206.12-P NL

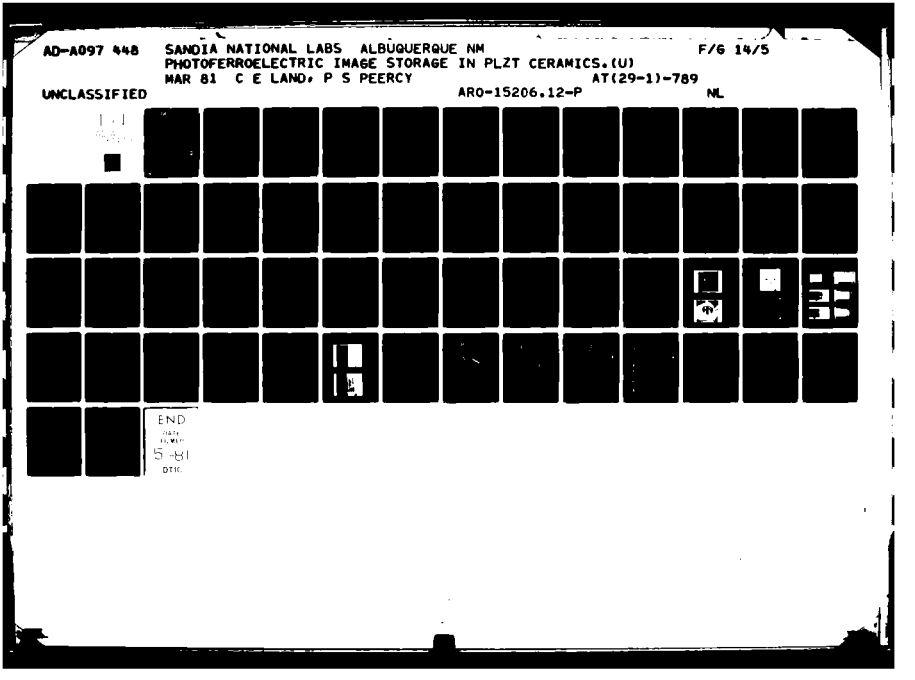

END
DATE FILMED
5-81
DTIC

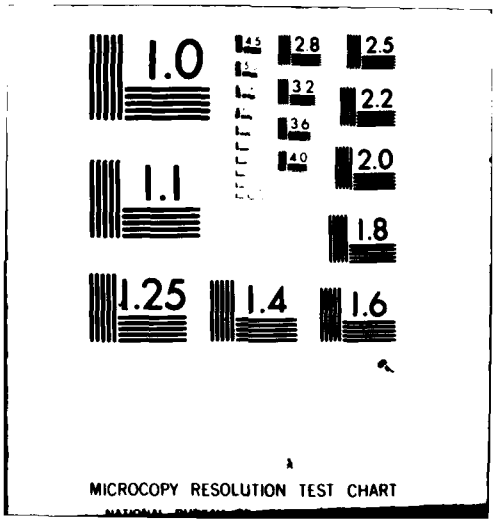
1.0
1.1
1.25
1.4
1.6
1.8
2.0
2.2
2.5
2.8
3.2
3.6
4.0
MICROCOPY RESOLUTION TEST CHART

LEVEL II

(11) ARO 15206.12-P

(14)

(12)

AD A097448

(6) PHOTOFERROELECTRIC IMAGE STORAGE IN PLZT CERAMICS.

(9) FINAL REPORT. F.1-78 - F 51

(10) CECIL E. LAND AND PAUL S. PEERCY

(11) MARCH 1981 (12) 57

SUBMITTED TO:

U. S. ARMY RESEARCH OFFICE (15) AT(27-1-2
RESEARCH TRIANGLE PARK, NC

ARO PROPOSAL NUMBER: 15206-P
1L161102 BH 57-07 PHYSICS

(16) (17)

SUBMITTED BY:

SANDIA NATIONAL LABORATORIES
ALBUQUERQUE, NM 87185

APPROVED FOR PUBLIC RELEASE
DISTRIBUTION UNLIMITED

21-30

THE FINDINGS IN THIS REPORT ARE NOT TO BE CONSTRUED AS AN OFFICIAL DEPARTMENT OF THE ARMY POSITION, UNLESS SO DESIGNATED BY OTHER AUTHORIZED DOCUMENTS.

FOREWORD

Since 1976 we have studied the mechanisms of photoferroelectric (PFE) image storage in lead lanthanum zirconate titanate (PLZT) ceramics. For the past three years, this study has been partially supported by the U.S. Army Research Office. The results of this study include: (1) demonstration of techniques for contrast inversion and contrast modification of images stored in ferroelectric (FE)-phase PLZT, (2) substantial increase of the contrast (optical density) range of stored images by using antiferroelectric (AFE)-phase PLZT as the image storage medium, (3) increase by a factor of ~ 10^4 of the PFE image storage sensitivity by ion implantation in FE-phase PLZT, and (4) derivation of a phenomenological model describing PFE image storage in both unimplanted and ion-implanted PLZT.

This report is divided into two major parts: (1) a description and discussion of the important results achieved thus far in this study, and (2) a discussion of specific objectives for future study which may lead to further significant developments in optical information storage and processing devices and technology. Specific objectives proposed for future study include: (1) further improvements of PFE image storage sensitivity by ion implantation in both ferroelectric - and antiferroelectric-phase PLZT compositions, (2) investigation of the possibilities for similar improvements of holographic storage sensitivity by ion implantation in psuedo-cubic, penferroelectric-phase PLZT compositions, (3) investigation to determine if further improvements can be achieved in photographic imaging charactistics, including higher storage and erasure speeds, increased contrast and resolution of stored images and increased photosensitivity to visible light of all types of PLZT compositions, and (4) investigation of PLZT device performance for specific applications.

TABLE OF CONTENTS

LIST OF ILLUSTRATIONS

LIST OF ILLUSTRATIONS (Continued)

1. STATE OF THE ART: PLZT PHOTOFERROELECTRIC IMAGE STORAGE

1.1 Introduction

We first demonstrated in 1976 that photographic images can be stored in transparent PLZT ceramics by exposure to near-UV light with photon energies equal to or greater than the band gap energy of ~ 3.35eV.[1] The image storage process relies on optically-induced changes in the switching properties of ferroelectric domains, i.e., the intrinsic photoferroelectric PFE effect.[1-3] Stored images are nonvolatile but can be erased by spatially uniform near-UV illumination and simultaneous application of an electric field. For the past three years[4] our study of PFE effects in PLZT has concentrated on four areas: (1) techniques for enhancing the contrast in selected areas of a stored image,[5,6] (2) increasing the contrast or optical density range of stored images,[7] (3) increasing the photosensitivity of the image storage process for ferroelectric(FE)-phase PLZT compositions by ion implantation,[8-13] and (4) deriving a phenomenological model to describe PFE image storage in both unimplanted and in ion-implanted FE-phase PLZT compositions.[11-13] Details of the results of this study are included in the following sections of this proposal.

1.2 PFE Device Configuration

PFE image storage devices are extremely simple and easy to fabricate. A device consists merely of a thin optically polished plate of PLZT with transparent indium-tin oxide (ITO) electrodes sputter-deposited onto the two major faces as shown in Fig. 1. The ITO electrodes have a thickness of ~ 0.12 μm and a sheet resistivity of ~ 10Ω/□.

For the ion-implanted devices, a 300 keV Accelerators, Inc. positive ion accelerator has been used for implantation. To achieve ion energies greater than 250 keV, doubly-charged ions were implanted. Initially, ions were implanted before the electrodes were deposited; however, we have recently found that more spatially uniform implants, and correspondingly more uniform domain switching, is obtained if a thin ($\leq$ 200Å) ITO layer is deposited prior to implantation to prevent charge buildup during implantation. A schematic illustration of the ion-implanted device is shown in Fig. 2. Typical device dimensions are 25 x 25 x 0.25 mm, although devices with much larger areas can be readily fabricated. Typical implant and absorption depths are $x_3 < 1$ µm and $x_2 \sim 10$µm, respectively, and the remaining thickness $x_1 \sim 240$µm is unaffected by either the implantation or the illumination.

1.3 Image Storage and Contrast Enhancement in Fe-Phase PLZT

Nonvolatile images with contrast ranges extending from an optical density of ~ 0.6 to > 2.6 and with resolution as high as 40 line pairs per millimeter are routinely stored in FE-phase PLZT using the intrinsic PFE effect. Photographs of two images stored in unimplanted PLZT are shown in Fig. 3. An example of the resolution achievable is given by the image of a resolution chart stored in Fig. 4. The photographs in this figure further illustrate the capability for altering images in PLZT after they are stored by the application of an external voltage. The photograph on the left is the image as stored whereas the photograph on the right shows the negative obtained by switching the remanent polarization after the image was stored. This switching is accomplished by the application of an appropriate voltage in the absence of UV illumination.

With the appropriate choice of the applied voltage, the contrast in regions of the image exposed at any given level can be enhanced as illustrated by the photographs in Fig. 5. Figure 5A is a photograph of the step density transparency used to store the image of Fig. 5B. The calibrated density variation is 0.5 optical density per step. The average remanent polarization P_r of the ceramic of Fig. 5B was arbitrarily set at zero for reference purposes. When P_r was switched to $-6.53\ \mu C/cm^2$, the maximum density step moved from position 1 in Fig. 5B to position 2 in Fig. 5C. As P_r was switched to increasingly negative values as shown in Figs. 5D, 5E, and 5F, the maximum density step moved from position 2 to positions 3, 4, and 5, respectively. This technique of baseline subtraction in the stored image may be used to modify and enhance the contrast of images stored in a PFE device.

In FE-phase PLZT, images are stored as spatial variations of light scattering centers; hence the contrast or optical density(OD) range of stored images is determined by the maximum and minimum scattering states.[14] In rhombohedral-phase PLZT 7/65/35, a solid solution with the composition

$$Pb_{0.93}\ La_{0.07}\ (Zr_{0.65}\ Ti_{0.35})_{0.983}\ O_3\ ,$$

the contrast range of stored images is about 2.0 OD, extending from a minimum scattering state at saturation remanent polarization ($P = \pm P_R$) of about 0.6 OD to a maximum scattering state near zero remanence ($P \cong 0$) of $\gtrsim$ 2.6 OD.[14] We have demonstrated that the contrast range of stored images can be substantially increased to about 3.0 OD by storing images in a PLZT 7.7/70/30 material which has coexisting AFE and FE phases.[7] In this material

images are stored as spatial variations of electric-field-induced, metastable FE (scattering)-phase in an initially nonscattering AFE-phase material. Images stored in the PLZT 7.7/70/30 material are nonvolatile, but they can be totally or selectively erased by uniformly illuminating the area to be erased with near-UV light and simultaneously applying a voltage of opposite polarity to the image storage voltage.[7] The increased contrast range of images stored in AFE-phase material indicates that this material may ultimately replace FE-phase PLZT as a PFE image storage medium.

1.4 Effects of Ion Implantation and Characteristics of the Ion-Implanted Region

While the use of PLZT for either temporary or long term image storage has many attractive features including manipulation of the stored image for contrast enhancement, the relatively large exposure energy W_{ex} of 100 to 300 mJ/cm^2 required to store high quality images has severely limited the applications of PLZT. We have now found that W_{ex} can be reduced dramatically by about four orders of magnitude when the electrical and dielectric properties of the near-surface region are altered by ion implantation. The ion implantation-induced photosensitivity enhancement results from the disorder produced by energy the implanted ions deposit into atomic collision processes, i.e., energy imparted to atomic nuclei of the PLZT by implanted ions. The primary effects of the disorder are to decrease the dielectric constant and the dark conductivity of the implanted region relative to the unimplanted dielectric constant and conductivity and to alter the photoconductivity of the implanted region. The substantial reduction of the dielectric constant indicates that the implanted region is probably no longer ferroelectric. The decrease in dark conductivity accounts for the observed increase in voltage required to switch the ferroelectric polarization. The large

voltage drop across the thin implanted layer (x_3 in Fig. 2) produces an extremely high drift field which results in a substantial increase in the number of photoexcited carriers swept into the absorption region x_2 at low illumination intensities.

The depth distribution of implanted ions and the depth distribution of energy deposited into atomic and electronic processes can be accurately calculated using codes developed by Brice.[15] Examples of the results of these calculations for 200 keV H and 200 keV He are shown in Figs. 6 and 7, respectively. The curves in Fig. 6 yield a projected range of 1.03 μm for 200 keV H and the maximum in the energy deposited into atomic processes occurs at 0.9 μm. The 200 keV H implants deposit $\lesssim$ 0.5% of the ion energy into atomic processes. For the more massive He ions, the projected range is 0.77 μm and the maximum of the energy deposited into atomic processes occurs at ~ 0.7 μm. For a given implant energy, the range of heavy ions decreases with increasing mass, but the fraction of implant energy deposited into atomic processes increases with increasing mass. This behavior is further illustrated in Figs. 8 and 9 for 500 keV Ne and 500 keV Ar implants, respectively. Since ion implantation-produced photosensitivity enhancement also depends on the thickness of the implanted layer, as will be discussed below, we have used co-implants of Ar and Ne to extend the disordered region to a depth of ~ 0.5 μm as shown in Fig. 10.

The dramatic increase in photosensitivity afforded by ion implantation is illustrated by the photographs shown in Fig. 11. The lower half of each ceramic plate was implanted with H ions and the upper half was not implanted. Both the upper unimplanted and lower implanted regions of the surfaces were exposed identically (20 mJ/cm^2) during image storage. As can be seen from

the photographs, a high quality image is stored in the implanted region at exposure levels insufficient to store a detectable image in unimplanted PLZT. It should also be noted that no degradation in the image quality is observed in the implanted material; in fact, for uniform implants, the image quality is generally higher than that for unimplanted PLZT.

1.5 Effects of Ion Implantation on Switching Characteristics

A hysteresis loop for an unimplanted, unilluminated PLZT sample 0.25 mm thick is shown in Fig. 12. For this thickness, the threshold field for domain switching, $E_{th} \sim 3.5 \times 10^5$ V/m, occurs at an applied threshold voltage $V_{th} \cong 100$ V. The coercive field $E_{c,u} = 4.8 \times 10^5$ V/m, where the polarization is zero, occurs at a coercive voltage $V_{c,u} \cong 120$ V. The subscript u in these notations indicates that the sample is unimplanted, and the subscript i denotes that the sample is implanted. When a similar sample is implanted with 2×10^{16} 200 keV H/cm^2, the dark coercive voltage $V_{c,i}(0) \cong 160$ V as shown by curve 1 of Fig. 13. At this applied voltage, the electric field in the underlying unimplanted region of the sample is taken to be equal to E_c of the unimplanted PLZT, since we assume E_c is a constant of the material. This implies that $V_{c,i}(0) - V_{c,u}(0) \cong 40$ V is impressed across the implanted layer as a result of the decreased conductivity associated with implantation-produced disorder. For the Ar + Ne co-implanted sample, Fig. 14, the dark coercive voltage (curve 0) has been increased to $V_{c,i}(0) \cong 275$ V. The voltage drop across the implanted layer in this sample is $V_{c,i}(0) - V_{c,u}(0) \cong 155$ V. This difference illustrates the effect of the greatly increased disorder in the Ar + Ne-implanted sample relative to that of the H-implanted sample. The curves numbered 1 through 15

of Fig. 14 were taken with increasing intensity I of near-UV illumination ranging from 1 $\mu W/cm^2$ (curve 1) to 98 mW/cm^2 (curve 15). The decrease in V_c with I is used for quantitative measurement of the photosensitivity as discussed below.

To store an image in the sample of Fig. 14, a switching voltage of, e.g., 150 V, would be applied to the ceramic in the absence of illumination. Since this voltage is less than the threshold voltage for domain switching, no FE domains would be reoriented. The image to be stored would then be exposed on the implanted surface using near-UV light. As can be seen from the data in Fig. 14, the simultaneous application of UV light and the switching voltage will reorient domains under the exposed regions of the ceramic. Since the domain switching is proportional to I, an image which faithfully reproduces the gray scale will be stored in the ceramic plate.

1.6 Phenomenological Model of the PLZT Photoferroelectric Effect

In this section we present a simple phenomenological model[4] to describe both the photoinduced reduction of V_c which governs the storage process and the ion-implantation enhancement of the photosensitivity. Since the photon energy is greater than the bandgap energy, the light will generate charge carriers and increase the conductivities in regions (2) and (3) of Fig. 2. To simplify the analysis, we first consider the case for unimplanted PLZT for which $x_3 = 0$ and $d = x_1 + x_2$. At the instant the voltage V is applied ($t = 0$), the electric fields in regions (1) and (2) are governed by

$$D_1 = D_2, \text{ or } \varepsilon_1 E_1 = \varepsilon_2 E_2 \quad , \tag{1}$$

where D_1, D_2 are electric displacements and ε_1, ε_2 are relative dielectric permittivities. For $t \to \infty$, the continuity equation reduces to

$$j_1 = j_2, \text{ or } \sigma_1 E_1 = \sigma_2 E_2 \quad , \tag{2}$$

where j_1, j_2 are current densities for regions (1) and (2), respectively, and σ_1, σ_2 are conductivities. For the experiments under consideration. we are interested in the long time (essentially dc) behavior governed by Eq. (2).

To estimate the effect of illumination on the conductivity σ_2, we assume that the photoexcited carrier concentration is dominated by intrinsic photoconductivity. Under this assumption the light-induced electron concentration N will obey

$$dN/dt = aI - bN^2 \tag{3}$$

where aI and bN^2 govern carrier excitation and recombination, respectively. For constant I, $dN/dt = 0$, so that N, and the attendant changes in σ, are proportional to $I^{1/2}$. For intrinsic photoconductivity we thus write for region (2)

$$\sigma_2(I) = \sigma_1 + A\sqrt{I(x)} \quad , \tag{4}$$

where $I_{(x)} = I_o e^{-\alpha x}$. If the conductivity is dominated by one type of carrier, A is given by $A = (a/b)\,\varepsilon \cdot \mu$, where e and μ are the electronic charge and carrier mobility, respectively and a and b are defined by Eq. (3). It should be noted that $\sigma_2(I)$ is an exponentially decreasing function of depth x from the surface with a fall-off governed by the absorption length α^{-1} of ~ 10 μm for λ = 365 nm.

The applied voltage V is dropped across the sample according to

$$V = \int_o^{x_2} E_2(x)dx + \int_{x_2}^{d} E_1 dx \qquad (5)$$

which, under the above assumptions, can be solved to yield the electric field through the sample, as

$$V_u(I) = E_1 d \left\{ 1 + \frac{2}{\alpha d} \ell n \left[\frac{\sigma_1 + A\sqrt{I_o} \exp(-\alpha x_2/2)}{\sigma_1 + A\sqrt{I_o}} \right] \right\} \qquad (6)$$

when the field E_1 is taken to be constant throughout region (1). The subscript u denotes unimplanted PLZT, and I_o is the light intensity at the surface. We could have written a general expression for E(x) throughout depth d and solved Eq. (5) to yield an equation identical to Eq. (6) with x_2 replaced by d. However, the purpose of dividing d into the regions x_1 and x_2 was to permit the solution to be expanded for small x_2, where x_2 is the depth for which $\sigma_2 >> \sigma_1$. Although this expansion requires an additional fitting parameter, the resulting equations are valuable for optimizing the device performance. We thus expand Eq. (6) for small x_2 to yield

$$V_u(I) \cong \left[1 + \left(\frac{\sigma_1}{\sigma_1 + A\sqrt{I_o}} \right) \frac{x_2}{x_1} \right] E_1 x_1 \quad . \qquad (7)$$

Two interesting features are evident from Eq. (7). Since I decreases rapidly with x, the depth x_2 over which there is an appreciable change in

σ changes with I. Secondly, in the above approximation, light-induced changes in the conductivity in region (2) have a second-order effect on the voltage required to attain a given field in the dark region (1). Physically this dependence reflects the fact that the low-conductivity bulk region governs the current through the sample. Once the conductivity of region (2) appreciably exceeds that of region (1), further increases in the conductivity of region (2) have only a small effect on the total current. Assuming that Eq. (7) holds at the coercive field for the present experimental conditions and postulating that the depth x_2 is governed by an equation similar to Eq. (4), within the framework of the above approximations Eq. (7) becomes

$$V_{c,u}(I) = E_{c,u}(0)d\left(1-\frac{x_2}{d}\right)\left[1+\left(\frac{x_2}{d-x_2}\right)\left(\frac{\sigma_1}{\sigma_1+A\sqrt{I_o}}\right)\right]$$

$$\tilde{=} V_{c,u}(0)\ (1-B\sqrt{I_o})\left[1+\frac{B\sqrt{I_o}}{1+A\sqrt{I_o}/\sigma_1(0)}\right] , \qquad (8)$$

where the approximate form of Eq. (8) derives from setting $x_2/(d-x_2) = x_2/d \equiv B\sqrt{I}$ in the second-order term. The subscript c denotes that $V_u(I)$ is evaluated at the coercive field $E_{c,u}$, and $E_{c,u}(0)$ is taken to be a constant parameter of the material, i.e., we assume a critical field is required to switch the unilluminated ceramic. B is defined by B = 1/d times a parameter analogous to A in Eq. (4). The physical significance of B is that $B\sqrt{I}$ is the value of x_2/d for which $E_2 \ll E_1$.

We next consider the effect of ion implantation. Ion implantation changes ϵ and σ in a well-defined near-surface ($\leq$ I μm) region denoted as

(3) in Fig. 1 and can have a marked effect on V_c for both the illuminated and the unilluminated conditions. Straightforward solution of equations analogous to Eqs. (2) and (5) for I = 0 yields

$$V_i(0) = \left(1 + \frac{\sigma_1}{\sigma_3(0)} \frac{x_3}{x_1}\right) E_1 x_1 \quad , \tag{9}$$

where the subscript i denotes implanted PLZT, and σ_3 is taken to be uniform over the depth x_3. From Eq. (9) it is apparent that the increase in the coercive voltage $V_{c,i}$ at I = 0 produced by ion implantation results from a decrease in the dark conductivity σ_3 (0) of region (3). For example, for 5×10^{14} 400 keV Ar/cm^2, which has $x_3 \cong 0.5$ μm, we find that $\sigma_1/\sigma_3(0) \cong 340$.

For I ≠ 0, if we approximate the sample by three regions, analogous to a two-region approximation for unimplanted PLZT, Eq. (2), (4), and (5) can be extended and solved to yield $V_{c,i}(I)$ in terms of the dark coercive field of region (1), $E_{c,u}(0)$. Assuming that the photoconductivity is intrinsic in the implanted region also, one finds

$$V_{c,i}(I) = V_{c,u}(I) + V_{c,u}(0)(1-B\sqrt{I_o}) \left(\frac{1}{1+ C\sqrt{I_o}/\sigma_3}\right)\frac{\sigma_1 x_3}{\sigma_3 x_1} \tag{10}$$

where $V_{c,u}(I)$ is given by Eq. (8) and C is analogous to A in Eq. (4) but refers to implanted material.

If the microscopic parameters such as a, b, μ etc., were known for PLZT, the parameters A, B and C introduced above could be evaluated to calculate $V_c(I)$ from first principles. Unfortunately, the microscopic parameters are not known, so we treat the parameters A, B and C in Eqs. (8) and (10) as adjustable parameters to determine if the intensity

dependence of V_c is adequately described by the model. $V_c(0)$ is directly measured at I = 0 and the parameters A and B in Eq. (8) can be readily evaluated from the data. The solid curve for the unimplanted sample in Fig. 15 was calculated for: $A/\sigma_1(0) = 2.0$ $(mW/cm^2)^{-1/2}$ and $B = 0.022$ $(mW/cm^2)^{-1/2}$. As can be seen for Fig. 15, Eq. (8) gives a good fit to the measured $V_{c,u}(I)$ for unimplanted PLZT throughout the intensity region 1 $\mu W/cm^2 \leq I \leq 100$ mW/cm^2 investigated.

Two variables of Eq. (10) which depend directly on the conditions of ion implantation are x_3 and q_3. To maximize photosensitivity, Eq. (10) indicates that the ion damage depth x_3 should be increased and that the dark conductivity $\sigma_3(0)$ in the implantation region should be minimized. The damage depth x_3 is increased either by implanting ions with lower mass or by implantation at higher energies; $\sigma_3(0)$ is reduced by maximizing implantation damage with more massive ions. Both of these dependences have been verified experimentally. The photosensitivity increase obtained with 500 keV Ar compared to 400 keV Ar (Fig. 15) illustrates the x_3 dependence. The lower photosensitivity for 200 keV He,[10] which has greater x_3 than does 500 keV Ar, reflects the damage dependence.

To describe the dependence of the coercive voltage on I for ion-implanted PLZT, we use the parameters obtained for unimplanted PLZT together with $\sigma_1 x_3 / q_3 x_1$ evaluated from Eq. (9) at I = 0 and C of Eq. (10) evaluated at some point on the $V_{c,i}(I)$ curve. Calculated $V_c(I)$ dependences for H, Ar, and Ar + Ne implants are compared with the measured dependences in Fig. 15. It is apparent from the curves in Fig. 15 for ion-implanted PLZT that Eq. (10) gives a reasonable description throughout the five decades in I which were measured. The curves for the Ar implants were

calculated using the above parameters and $C/\sigma_3(0) = 0.80\ (mW/cm^2)^{-1/2}$. Identical parameters were used for the 400 and 500 keV Ar implants, with the exception of x_3 which was adjusted to account for the calculated differences in range of the implants.[15] The fact that both curves give accurate fits to the data lends further support for this model.

The ion-implantation induced enhancement in photosensitivity is summarized in Fig. 16 where the change in coercive voltage ΔV_c is plotted as a function of I for different implanted ions. Empirically we find that the image storage threshold for a one-second exposure occurs at $\Delta V_c \sim -25V$, independent of the implanted species. The image storage threshold may thus be read directly from the curves in Fig. 16, and has been decreased from $\sim 85\ mJ/cm^2$ in unimplanted PLZT to $\sim 45\ \mu J/cm^2$ for co-implants of 5×10^{14} 500 keV Ar + 1.5×10^{15} 400 keV Ne. Very recently, we have further reduced the threshold energy to $\sim 10\ \mu J/cm^2$ with co-implants of 500 keV Ne and 350 keV Ar which yields a more uniform damage distribution than the co-implants reported in Fig. 16. We should also note that implantation with chemically active ions can be used to shift the absorption spectrum so that visible light can be used for image storage. For example, preliminary measurements indicate that light from an incandescent source can be used to store high quality images in Al-implanted PLZT. The measured photosensitivity for a sample implanted with 1×10^{15} 500 keV Al/cm^2 is decreased by less than an order of magnitude at 436 nm compared to the photosensitivity at 365 nm.

1.7 Conclusions

Within the past three years major advances have been made in understanding the physics of the intrinsic photoferroelectric effects in PLZT

ceramics. Physical properties which have important potential applications have been investigated. It has been found, for example, after storage of an optical image in a FE-phase PFE device, that the sense of the image can be inverted from a positive to a negative, or vice-versa. The contrast of a stored image can be varied arbitrarily by switching the FE remanent polarization to values intermediate to those which produce a positive or negative image.[5,6] These properties can be used to achieve contrast enhancement in selected areas of a stored image. The contrast range of images stored in FE-phase PLZT is typically about 0.6 to 2.6 OD. By storing images in a PLZT composition with coexisting AFE and FE phases, the contrast range of stored images has been increased typically to about 0.3 to 3.3 OD. This permits storage of images with substantially increased gray scale in the AFE-phase PLZT.[7]

Prior to this work, the relatively low photosensitivity associated with PFE image storage in unmodified PLZT constituted a serious disadvantage for most information storage and display applications. By implanting inert gas ions into the surface of FE-phase PLZT, the photosensitivity of the PFE image storage devices has been increased by about four orders of magnitude.[12,13] The exposure energy at the image storage threshold is ~ 10 $\mu J/cm^2$ for Ar + Ne co-implanted PLZT compared to ~ 100 mJ/cm^2 for unimplanted material. With this remarkable increase in photosensitivity, FE-phase PLZT is now the most sensitive, nonvolatile, selectively-erasable image storage medium known to exist. Several important properties of various image storage media are listed in Table I. From the data given in the table, it is apparent that ion-implanted PLZT has about the same photosensitivity as $Bi_{12}Si_{20}$ PROM devices, but the PLZT has the advantages

of nonvolatile storage and appreciably larger maximum image storage area. These factors may be quite important for several memory and display applications.

2. OBJECTIVES FOR FUTURE WORK

2.1 Ion Implantation in Ferroelectric-Phase PLZT

Ion implantation in FE-phase PLZT has produced recent dramatic improvements in PFE imaging photosensitivity and has led to significant advances in the understanding of the image storage mechanisms involved.[10-13] The model presented in section 1.6 clearly indicates that the photosensitivity can be further improved by increasing the depth x_3 of the damage profile and by minimizing the dark conductivity $\sigma_3(0)$ of the implanted region. Experimental evidence also indicates that uniform damage, both spatially and as a function of depth from the surface, is an important factor in reducing the value of $\sigma_3(0)$. We therefore propose to continue our experiments with multiple co-implants of inert gas ions in order to optimize the photosensitivity to near-UV light.

We propose to further refine the phenomenological model presented in section 1.6 in an effort to identify other factors which may contribute to increased photosensitivity of the FE-phase PLZT. Efforts will be made to measure photocarrier excitation and recombination coefficients (a and b of Eq. (3)) and carrier mobility μ in the implanted layer. If experimental techniques can be developed to evaluate these variables, the photoconductivity coefficients A, B, and C of Eqs. (8) and (10) can be calculated directly from first principles. We propose to perform ion back-scattering experiments to verify calculations of the depth profile of the disorder produced by

ion implantation. The results of these experiments should lead to further refinements of the implantation parameters and increased near-UV photosensitivity.

In an effort to shift the absorption edge of the implanted layer into the visible, we propose to perform co-implants of chemically active ions into the FE-phase PLZT. The rationale for increasing the photosensitivity to visible light is to obtain a medium capable of storing images with illumination from common light sources such as incandescent and fluorescent lamps and, hopefully, sunlight. Preliminary results of our first experiments with Al implants (see section 1.6) indicate that chemically active ion implantation may provide the means of obtaining photosensitivites with visible light which approach or equal those obtained with near-UV light. We propose to evaluate the results of chemically active ion implantation by performing careful transmission spectra measurements on FE-phase PLZT samples which are unimplanted, implanted with inert-gas ions, and implanted with chemically active ions. The refined phenomenological model characterizing PFE effects will be applied to the chemically active ion-implanted PLZT to optimize the implantation parameters.

2.2 Ion Implantation in Antiferroelectric-Phase PLZT

We have demonstrated that images stored using the PFE effect in AFE-phase PLZT have a substantially increased contrast range compared to images stored in FE-phase material.[7] We therefore propose to investigate ion implantation in AFE-phase PLZT compositions as a means of achieving photosensitivities in these materials which are comparable to those of ion implanted FE-phase PLZT.

Since the PFE image storage processes in AFE-phase PLZT differ substantially from those in FE-phase material, we propose to develop a phenomenological model which characterizes the PFE effects in the AFE-phase. This model will be used to optimize the ion implantation parameters for AFE-phase material which should lead to greatly improved photosensitivity to both near-UV and visible light. Experiments similar to those described in section 2.1 will be performed to characterize the physical effects of ion implantation and to optimize the image storage properties of the AFE-phase PLZT.

2.3 Ion-Implantation in Penferroelectric-Phase PLZT

In 1972, Micheron, et al.[16] reported that they had stored holograms in FE-phase PLZT X/65/35, with X = 2, 5 and 7, using the photorefractive effect or photoinduced changes in refractive index (PCI). They and others have since studied PCI extensively in psuedo-cubic, penferroelectric (PEN) - phase[17] PLZT X/65/35, with x = 9 and 10, and they have stored holograms with diffraction efficiencies as high as 0.20 in these materials.[18-24] All of these experiments were performed using visible light at the argon laser wavelength λ = 488 nm, hence they involved the extrinsic photoferroelectric effect in PLZT. Although the resolution and diffraction efficiencies reported were satisfactory for holographic storage, the photosensitivity of the PLZT was two to three orders of magnitude less than that required for practical holographic memories and image storage devices. Our experiments indicate that approximately one order of magnitude increase in photosensitivity is achieved by using the intrinsic photoferroelectric effect, i.e., decreasing the wavelength of the light to $\lambda \sim 365$ nm or less. Our initial experiments with image storage in Ar + Ne co-implanted

PLZT 9/65/35 material indicate that the photoferroelectric sensitivity is further increased by more than three orders of magnitude compared with unimplanted PLZT-9/65/35. If a similar increase in photorefractive sensitivity is produced by ion implantation, this material will be the most photosensitive erasable holographic storage medium known to exist.

In order to achieve the desired high-sensitivity, erasable holographic storage medium, we propose to conduct a detailed study of both inert gas and chemically-active ion implantation in PEN-phase PLZT ceramics. This study will involve the experimental determination of both intrinsic and extrinsic photorefractive sensitivities of unimplanted as well as ion implanted PEN-phase PLZT. We also propose to derive a model for the photorefractive sensitivity enhancement due to ion implantation. This model will be used to optimize holographic storage sensitivity in PEN-phase PLZT.

2.4 Improvement of Photoferroelectric Imaging Characteristics

2.4.1 Minimizing Image Storage and Erasure Times

Although the photosensitivity of FE-phase PLZT has been increased by about four orders of magnitude by ion implantation, the minimum times required for image storage have not yet been determined. The reason for this is that PFE image storage and erasure both involve two concurrent processes, i.e., photoexcitation of carriers into the conduction band by image light and FE domain reorientation by an applied electric field. It is likely that the theoretical limitation to minimum image storage and erasure times is governed by Eq. (10), which depends on carrier excitation and recombination coefficients and carrier mobility. However, from a

practical device standpoint, the limiting factor for image storage and erasure speed may be domain switching time.

The switching time t_s required for domain reorientation in ferroelectric materials depends on the magnitude of the switching field (the field E_1 in the bulk region (1) of Fig. 2) which is given by the following expression,[25]

$$t_s = t_o \exp (E_a/E_1), \tag{11}$$

where t_o is a constant and E_a is an activation field which is also a constant for $E_1 \leq 2E_{c1}$.[26] (E_{c1} is the coercive field of the bulk region (1) of Fig. 2.) For $E_1 > 2E_{c1}$, the switching time no longer follows an exponential law as in Eq. (11), but instead it follows a power law of the type

$$t_s = \kappa E_1^{-n} \tag{12}$$

where κ is a constant and n depends on the PLZT composition and the magnitude of E_1.[26] Although switching times as short as 10 ns have been achieved for similar ceramic FE-compositions by Plumlee,[27] switching fields of $E_1 \sim 10\ E_{c1}$ were required. Since strains accompanying domain switching are relatively large for FE-phase PLZT,[28] it is impractical to consider switching at such high field strengths for PLZT image storage devices. Ultimately the minimum t_s for image storage devices will be governed by the switching strain pulse which can be tolerated and by the carrier photoexcitation and mobility which can be achieved in the implanted layer.

We propose to determine experimentally the minimum practical image storage and erasure times for the most photosensitive ion-implanted FE-

and AFE-phase PLZT compositions. This will necessarily involve a study of how the switching characteristics of ion-implanted PLZT ceramics are affected by both near-UV and visible illumination. It will also require experimental determination of the limitations of the reciprocity law for image storage in ion-implanted PLZT. The reciprocity law for image storage is given by

$$W_{th} = It, \tag{13}$$

where W_{th} is the threshold exposure energy required to store an image with a contrast range of about one-tenth the maximum contrast for PLZT, I is the image light intensity, and t is the exposure time. The threshold exposure energies W_{th} for t = 1 second are indicated for unimplanted, H- He-, Ar- and Ar + Ne- co-implanted PLZT 7/65/35 in Fig. 16. The objective of the proposed study is to determine the minimum time t for which Eq. (13) holds for both near-UV and visible illumination. We then propose to adjust the ion implantation parameters to achieve minimum image storage and erasure times for FE-phase and AFE-phase PLZT compositions.

2.4.2 Improvement of Image Contrast Range

Light scattering in FE-phase PLZT ceramics results from the refractive index discontinuities at domain and grain boundaries. The contrast range of images stored in these materials is determined by the difference between the scattering (spatial broadening of an incident collimated beam) of transmitted light when the ceramic is in the fully-poled, saturation remanence state and when it is in the electrically depoled state.[14,29] To maximize the contrast range, it is necessary to control the ceramic

grain size in order to obtain minimum scattering in the saturation remanence state and maximum scattering in the electrically depoled state. Experiments indicate that this condition is obtained for some FE-phase compositions with an average grain size of about 5 μm.[30] We propose to conduct further experiments on FE-phase PLZT compositions to determine the optimum grain size and composition for maximum contrast range of stored images.

Previously published measurements of the contrast range of stored images have been made using a He-Ne laser as a light source. We propose to investigate contrast range as a function of light wavelength, since the refractive index, and consequently light scattering are dependent on wavelength.[31-33]

We also propose to investigate contrast range as a function of grain size and composition in AFE-phase PLZT in order to optimize these parameters to obtain maximum contrast range.

2.4.3 Improvement of Resolution

In both FE-phase and AFE-phase PLZT devices, the resolution of stored images is limited by the dimensions of the scattering centers. When the contrast range of stored images depends on spatial scattering of transmitted light, the optimum grain size of the ceramic appears to be about 5 μm, and the dimensions of the scattering centers probably range from 2 to 5 μm. For this condition, the dimensions which have been measured for a minimum resolution element are between 10 and 15 μm (50 and 33 line pairs/mm). The resolution, therefore, appears to be grain-size limited for this type of image storage device.

In addition to spatial scattering, incident light is also depolarized when it passes through a PLZT ceramic plate. Although spatial scattering is reduced as the grain size is decreased below 5 μm, depolarization

scattering becomes predominant at grain sizes below 3 μm. If depolarization scattering in 2-3 μm grain size ceramics has a dependence on ferroelectric remanent polarization similar to that of spatial scattering in 5 μm grain size ceramic, then it may be possible to improve resolution by as much as a factor of 2 by reducing grain size and using linear polarizers to view or project stored images. We propose to investigate the possibility of increasing image resolution by decreasing the average grain size of both FE- and AFE-phase PLZT ceramics.

We propose to investigate contrast of stored images as a function of spatial frequency of the image for varying average grain size and varying FE- and AFE- phase compositions. The effects of readout of light wavelength on both contrast ratio and resolution of stored images will also be determined.

Signal-to-noise (S/N) ratio is an important consideration for images stored in scattering mode devices. We propose to investigate improvement of S/N ratio in stored images as a function of the grain size of the PLZT ceramic.

2.5 Investigation of Device Performance for Specific Applications

2.5.1 Image Storage

Images stored in PLZT ceramics are nonvolatile but selectively erasable. The PFE image storage devices are suitable for temporary or intermediate image storage from transparencies or with proper illumination, direct image exposure. For storage of facsimile data transmitted over a communication channel, we propose to demonstrate the ability of the PFE devices to store image information in the form of an intensity-modulated

light beam scanned a line-at-a-time across the storage surface. To demonstrate this ability an initial experiment will be performed using an intensity-modulated, near-UV laser light source and galvanometer-type optical scanners for x- and y- beam deflection. Experiments will be designed to determine the difference between writing and erasure sensitivities.

We have previously demonstrated the ability of PFE image storage devices for contrast modification of stored images using baseline subtraction techniques. We propose further study of reprocessing of stored images to reveal details that can be obscured by noise or shadows, especially for images stored in AFE-phase PLZT ceramics.

2.5.2 Reflective-Mode Readout of Stored Images

When an image is stored in a PFE device, surface deformation strains form a relief pattern of the stored image.[14] Light reflected from the deformed surface is modulated by the surface deformations into a set of spatial frequencies characteristic of the stored image, which can be converted into an intensity-modulated reproduction of the image by Schlieren optics. For storage of optical masks, filters, and matrices and for incoherent-to-coherent image conversion, reflective-mode readout of stored images is required since light scattering is undesirable in these applications. The reflective-mode device differs from that shown in Fig. 1 in that a dichroic film which transmits in the blue, violet, and near-UV and reflects longer wavelength visible light is deposited over the transparent electrode on the image storage surface. We propose to investigate vacuum evaporation or sputter deposition of dichroic films to optimize reflective-mode readout of stored images.

2.5.3 Image Readout Using Nondestructive Line-at-a-time Scanning of the Stored Image

Micheron, et al[34] have demonstrated facsimile-type-nondestructive readout of images stored in a ferroelectric-photoconductor device using PLZT 7/65/35 as the storage medium. Images were read out as electrical signals at commercial television scan rates by measuring the current photoinduced by a deflected Argon Ion Laser beam in the absence of an applied field. This nondestructive direct optical-to-electrical image conversion capability is available in PFE image storage devices, and it can be employed for fast-scan, facsimile transmission of images over communication channels. We propose to perform experiments to demonstrate this capability of PFE devices and to investigate maximum frame rates for image transmission using these techniques.

2.5.4 Holographic Storage in Penferroelectric-Phase PLZT

The extensive investigations of Micheron and others[18-24] of holographic storage in PEN-phase PLZT (discussed in section 2.3) demonstrate the need for a nonvolatile, selectively-erasable holographic storage medium. Our initial experiments with ion-implanted PEN-phase PLZT indicate that photorefractive storage sensitivity required to make these devices practical can be achieved by using ion implantation. We propose to perform experiments involving holographic storage in ion-implanted material, and to evaluate the stored holograms in terms of diffraction efficiency and spatial resolution. This appears to be an important new practical application of the photoferroelectric effects in PLZT.

2.5.5 Aging and Lifetime Characteristics of PFE Devices

If the characteristics of specific PFE devices appear to meet the requirements of certain applications, we propose to develop and perform experiments which will determine aging effects and lifetime of those devices. The object of such experiments will be to detect the effects of aging as a function of the number of write-read-erase cycles experiments by the devices.

References

1. C. E. Land and P. S. Peercy, "New Image Storage Mechanisms in PLZT Ceramics Using Near-Ultraviolet Light," 1976 IEEE-SID Biennial Display Conf. Record, 71-75 (1976).
2. C. E. Land and P. S. Peercy, "Photoferroelectric Image Storage in PLZT Ceramics," Information Display J. 13, 20-26 (1977).
3. C. E. Land and P. S. Peercy, "Photoferroelectric Effects in PLZT Ceramics," Ferroelectrics 22, 677-679 (1978).
4. Work partially supported by the U. S. Army Research Office and the Research Institute of the U. S. Army Engineer Topographic Laboratories, ARO Project: 1L161102BH57-07 (Physics).
5. C. E. Land and P. S. Peercy, "Photoferroelectric Image Storage and Contrast Modification in PLZT Ceramics," 1978 SID Intl. Symp. Dig. of Tech. Papers 9, 14-15 (1978).
6. C. E. Land, "Optical Information Storage and Spatial Light Modulation in PLZT Ceramics," Optical Engineering 17, 317-326 (July-Aug. 1978).
7. C. E. Land, "Photoferroelectric Image Storage in Antiferroelectric-Phase PLZT Ceramics," 1978 IEEE-SID Biennial Display Research Conf. Record, 38-41 (Oct. 1978); also Special Joint Issue IEEE Trans. on Electron Dev. ED-26, 1143-1147 (Aug. 1979); and Proc. SID 20, 219-223 (1979).
8. C. E. Land and P. S. Peercy, "Ion Implanted PLZT for Photoferroelectric Image Storage and Display Devices," Ferroelectrics 27, 131-136 (1980).
9. C. E. Land and P. S. Peercy, "Enhanced Sensitivity of Photoferroelectric Image Storage in Ion-Implanted PLZT Ceramics," 1980 SID Intl. Symp. Dig. of Tech. Papers 11, 220-221 (April 1980).

10. C. E. Land and P. S. Peercy, "Photosensitivity Enhancement by H- and He-Ion Implantation in Lead Lanthanum Zirconate Titanate Ceramics," Appl. Phys. Lett. 37, 39-41 (July 1980).

11. P. S. Peercy and C. E. Land, "A Model for Ion-Implantation Induced Improvements of Photoferroelectric Imaging in PLZT Ceramics" Appl. Phys. Lett. 37, 815-818 (Nov. 1980).

12. P. S. Peercy and C. E. Land, "Optical Image Storage in Ion-Implanted PLZT Ceramics," Proc. Ion Beam Modif. of Matls. Conf. (to be published in Nuclear Instruments and Methods, 1981).

13. P. S. Peercy and C. E. Land, "Ion-Implanted PLZT Ceramics: A New High-Sensitivity Image Storage Medium," 1980 IEEE-SID Biennial Display Research Conf. Record, 133-139 (Oct. 1980); Also, to be published in Special Joint Issue IEEE Transactions on Electron Devices ED-28 (1981) and Proc. SID 22, (1981).

14. C. E. Land "Variable Birefringence, Light Scattering and Surface-Deformation Effects in PLZT Ceramics," Ferroelectrics 7, 45-51 (1974).

15. D. K. Brice, "Spatial Distribution of Energy Deposited into Atomic Processes in Ion-Implanted Silicon," Rad. Eff. 6, 77 (1970); Recoil Contribution to Ion Implantation Energy Deposition Distributions," J. Appl. Phys. 46, 3385 (1975).

16. F. Micheron, A. Hermosin, G. Bismuth and J. Nicolas, "Inscription de Reseaux Holographiques dans les Ceramiques Ferroelectriques Transparentes," C. R. Acad. Sci. Paris 274B, 361-364 (1972). (In French.)

17. A. H. Meitzler and H. M. O'Bryan, Jr., "Polymorphism and Penferroelectricity in PLZT Ceramics," Proc. IEEE 61, 959-966 (1973).

18. F. Micheron, C. Mayeux, and J. E. Trotier, "Electrical Control in Photoferroelectric Materials for Optical Storage," Appl. Optics 13, 784-787 (1974).

19. F. Micheron, J. M. Rouchon, and M. Vergnolle, "Optical Recording of Digital Data in PLZT Ceramics," Appl. Phys. Lett. 24, 605-607 (June 1974).

20. F. Micheron, C. Mayeux, A. Hermosin, and J. Nicolas, "Holographic Storage in Quadratic PLZT Ceramics," J. Am. Ceram. Soc. 57, 306-308 (1974).

21. J. M. Rouchon, M. Vernolle, and F. Micheron, "Photoinduced Changes of Refractive Index in PLZT Ceramics," Ferroelectrics 11, 389-392 (1976).

22. B. Houlier and F. Micheron, "Photoinduced Charge-Transfer Process in PLZT Ceramics," J. Appl. Phys. 50, 343-345 (1979).

23. F. Micheron, "Sensitivity of the Photorefractive Processes," Ferroelectrics 18, 153-159 (1978).

24. J. W. Burgess, R. J. Hurditch, C. J. Kirkby and G. E. Scrivener, "Holographic Storage and Photoconductivity in PLZT Ceramic Materials," Appl. Optics 15, 1550-1557 (1976).

25. W. J. Merz, "Domain Formation and Domain Wall Motions in Ferroelectric $BaTiO_2$ Single Crystals," Phys. Rev. 95, 690-698 (1954).

26. E. Fatuzzo and W. J. Merz, Ferroelectricity, North-Holland Publishing Co., Amsterdam (1967), Ch. 7.

27. Ralph H. Plumlee, "Ferroelectric Switching Time Measurements," IEEE Trans. on Instr. and Meas. IM-22, 231-234 (1973).

28. Peter J. Chen and C. E. Land, "Variations of Strain and Light Scattering Accompanying Domain Switching in Lead Lanthanum Zirconate Titanate Ceramics," J. Appl. Phys. 51, 4961-4966 (1980).

29. A. L. Dalisa and R. J. Seymour, "Convolution Scattering Model for Ferroelectric Ceramics and Other Display Media," Proc. IEEE 61, 981-991 (1973).

30. J. R. Maldonado and D. B. Fraser, "PLZT Ceramic Display Devices for Slow-Scan Graphic Projection Displays," Proc. IEEE 61, 975-981 (1973).

31. C. E. Land and P. D. Thacher, "Ferroelectric Ceramic Electrooptic Materials and Devices," Proc. IEEE 57, 751-768 (1969).

32. C. E. Land and P. D. Thacher, "Electrooptic Properties of Ba, Sn, and La Modified Lead Zirconate Titanate Ceramics," in The Physics of Opto-Electronic Materials, W. A. Albers, Jr., Ed., Plenum Publishing Corp., New York, (1971), pp. 169-196.

33. C. E. Land, P. D. Thacher and G. H. Haertling, "Electrooptic Ceramics," in Applied Solid State Science 4, R. Wolfe, Ed., Academic Press, Inc., New York (1974) pp. 137-233.

34. F. Micheron, J. M. Rouchon, and M. Vergnolle, "A Ferroelectric Image Memory," Ferroelectrics 10,. 15-18 (1976).

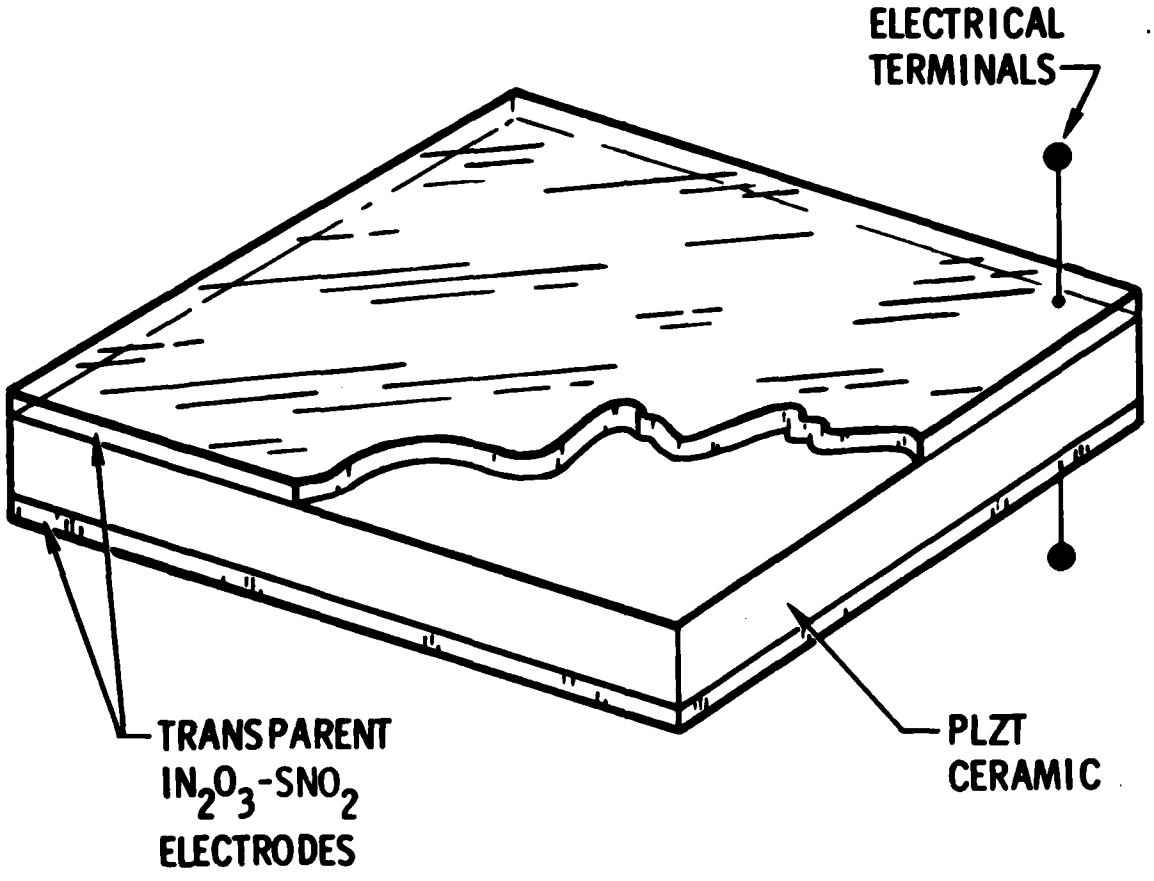
ELECTRICAL
TERMINALS
TRANSPARENT
IN_2O_3-SNO_2
ELECTRODES
PLZT
CERAMIC

Figure 1

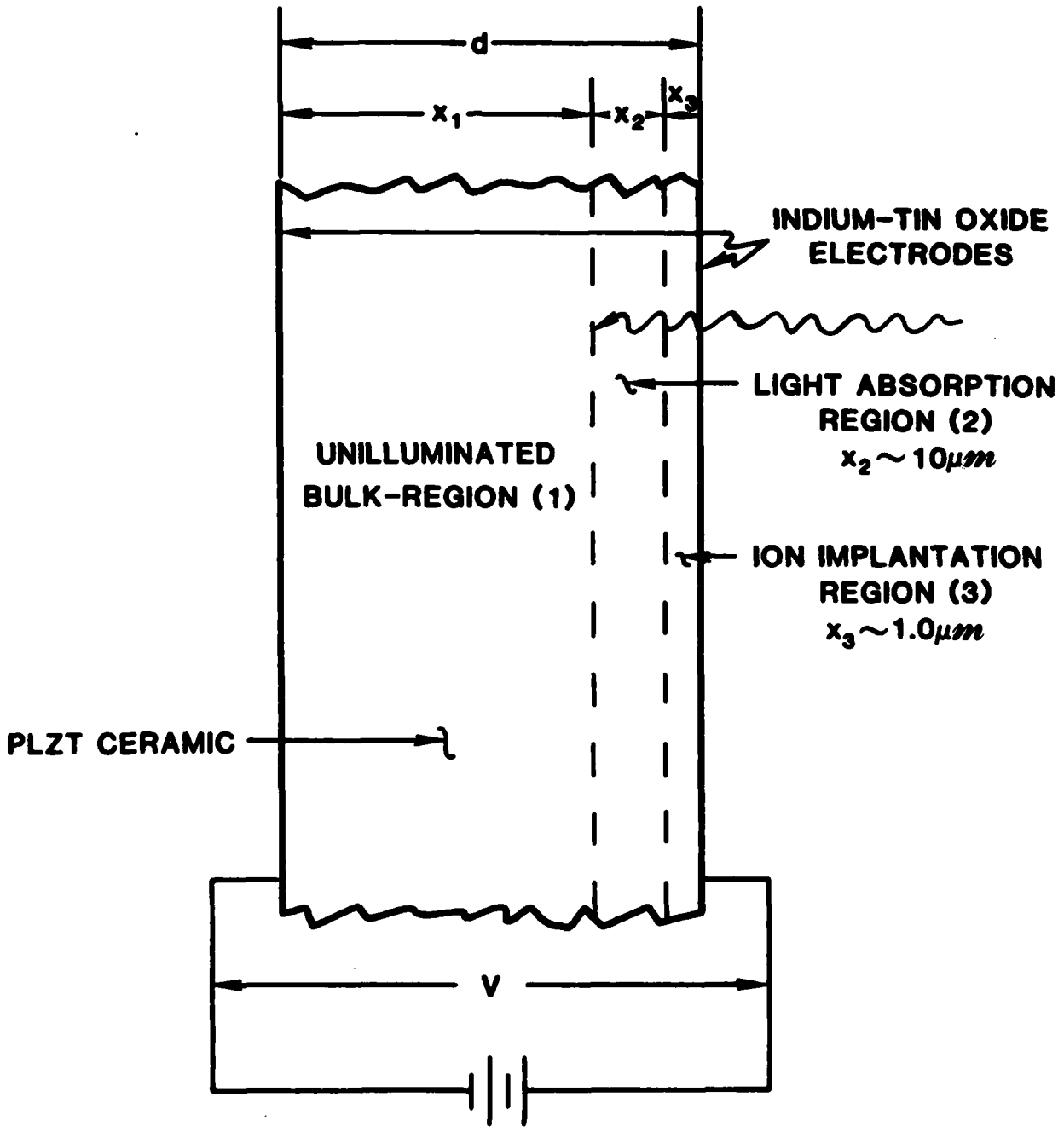
d
x_1
x_2
x_3
INDIUM-TIN OXIDE
ELECTRODES
LIGHT ABSORPTION
REGION (2)
$x_2 \sim 10\mu m$
UNILLUMINATED
BULK-REGION (1)
ION IMPLANTATION
REGION (3)
$x_3 \sim 1.0\mu m$
PLZT CERAMIC
V

Figure 2

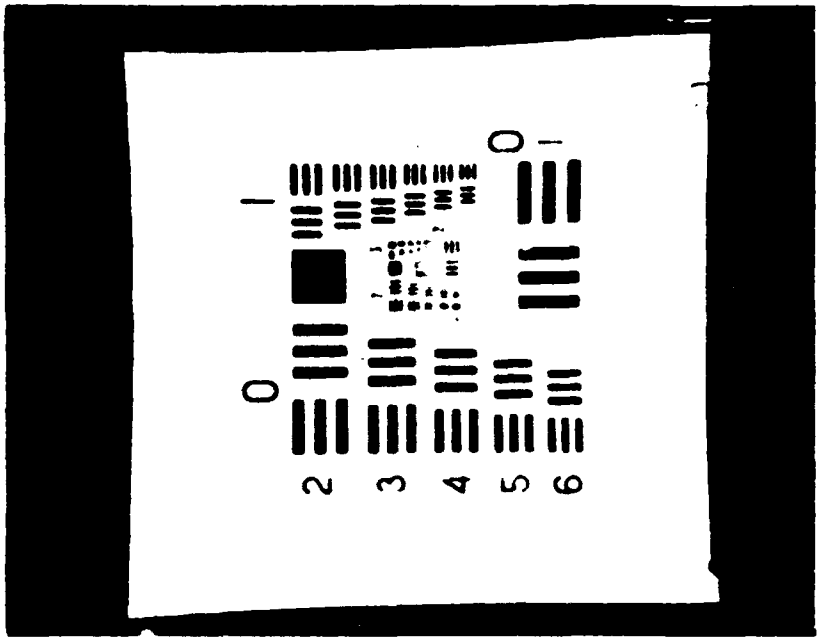

B

A

Figure 3

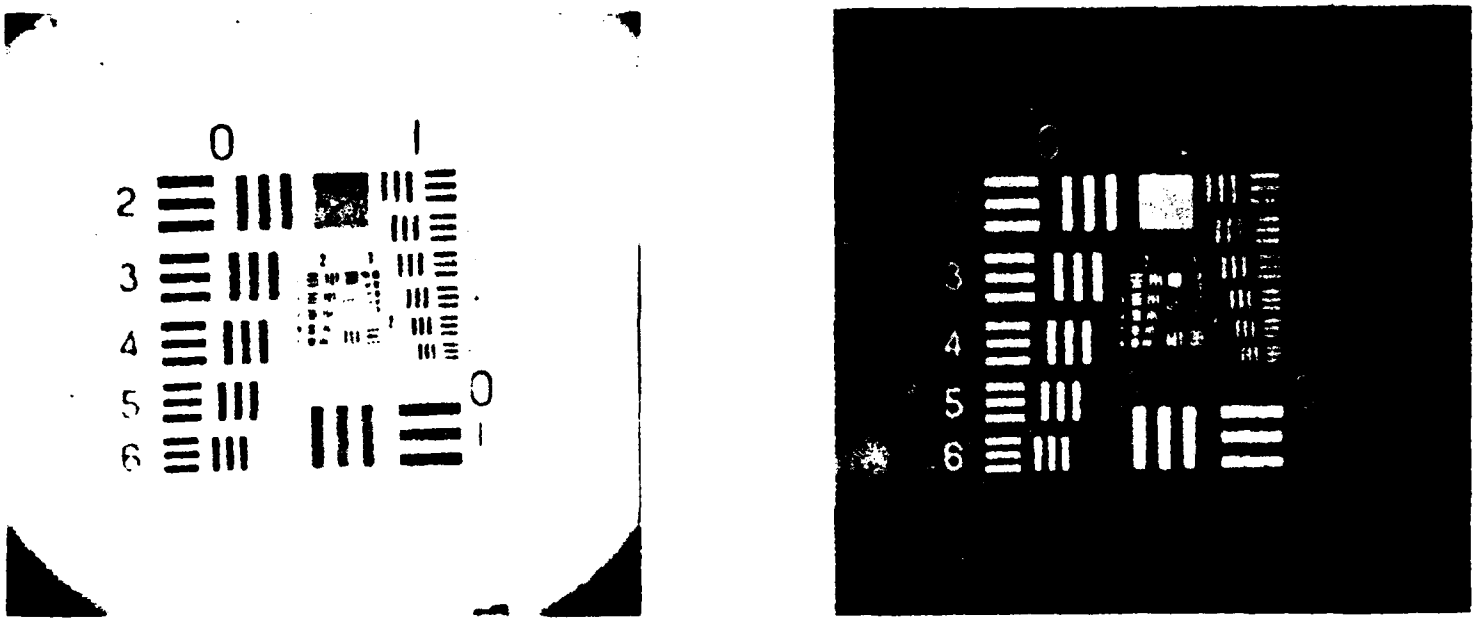

A B

POSITIVE-TO-NEGATIVE IMAGE CONVERSION IN PLZT 7/65/35. (A) POSITIVE IMAGE (NEGATIVE OF INPUT IMAGE), AND (B) NEGATIVE IMAGE OF (A).

Figure 4

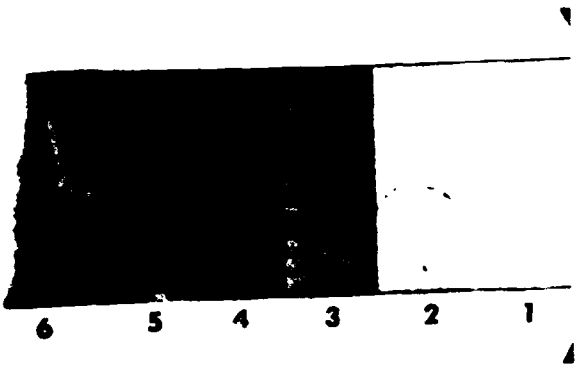

INPUT STEP DENSITY SCALE

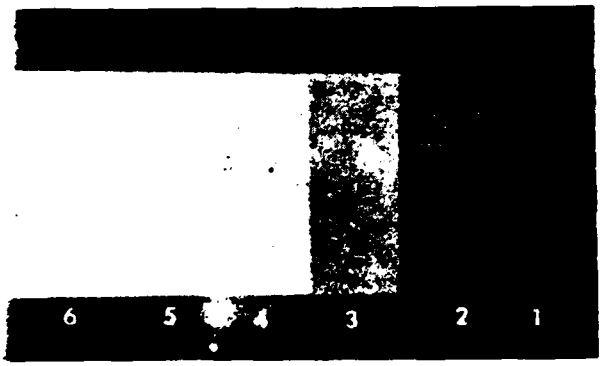

(B) STORED NEGATIVE OF (A)
$P_R(AV) = 0$

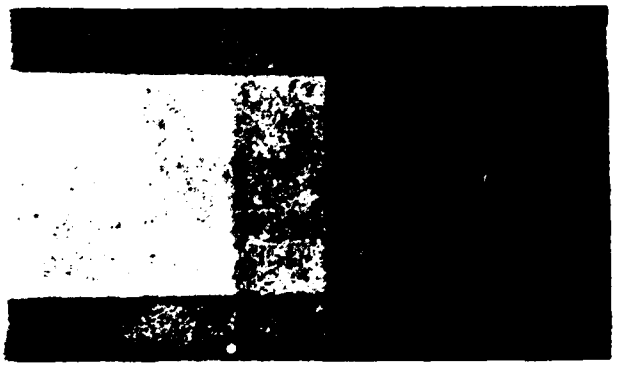

(C) IMAGE IN (B) AFTER SWITCHING TO $P_R(AV) = -8.53\ \mu C/CM^2$

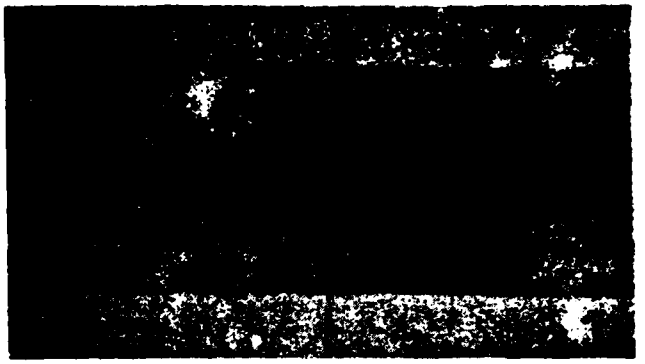

(D) IMAGE IN (B) AFTER SWITCHING TO $P_R(AV) = -12.30\ \mu C/CM^2$

(E) IMAGE IN (B) AFTER SWITCHING TO $P_R(AV) = -17.35\ \mu C/CM^2$

(F) IMAGE IN (B) AFTER SWITCHING TO $P_R(AV) = -21.56\ \mu C/CM^2$

Figure 5

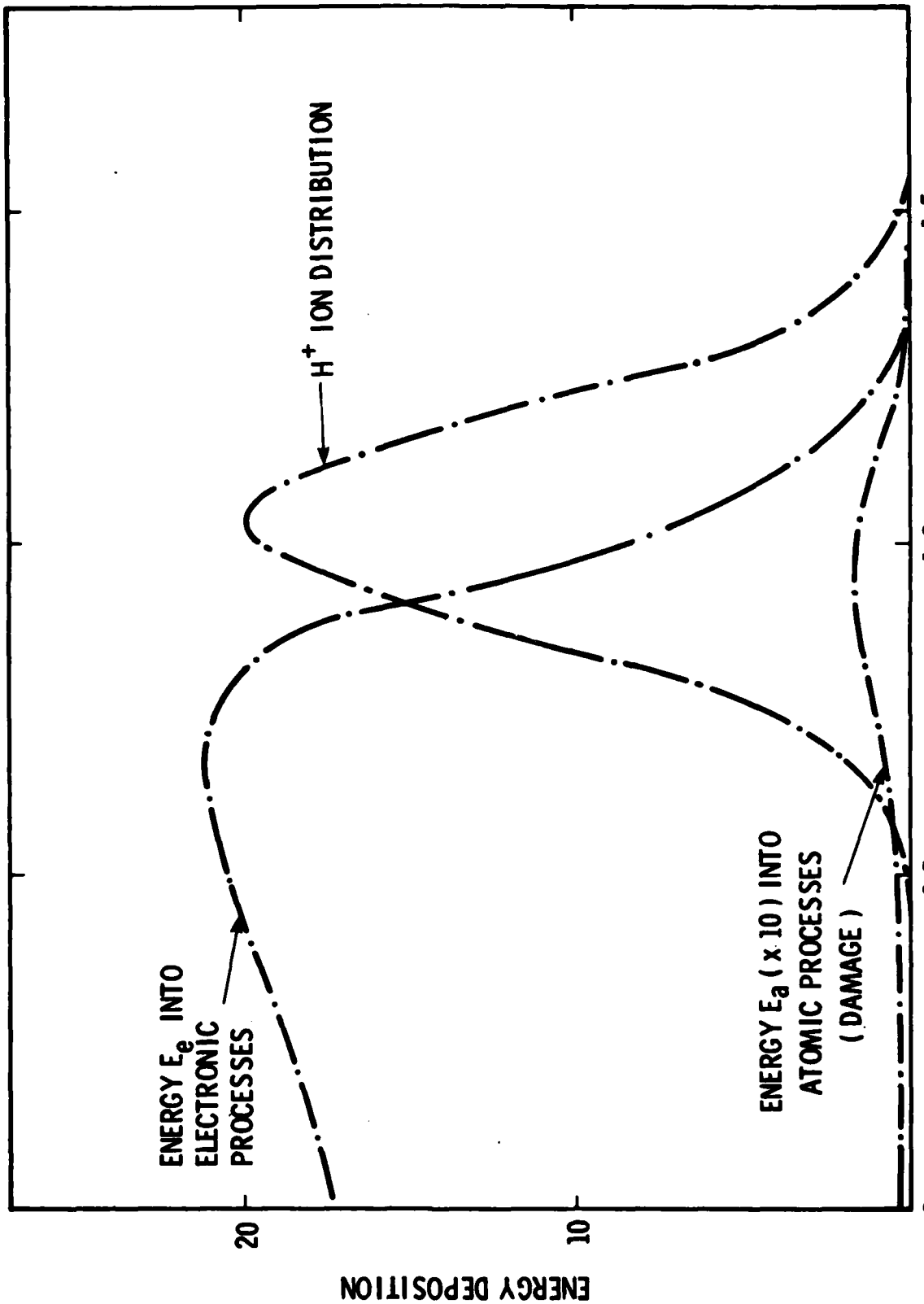
ENERGY DEPOSITION
20
10
0
0.5
1.0
1.5
DEPTH (μm)
H+ ION DISTRIBUTION
ENERGY Ee INTO ELECTRONIC PROCESSES
ENERGY Ea (x 10) INTO ATOMIC PROCESSES (DAMAGE)

Figure 6

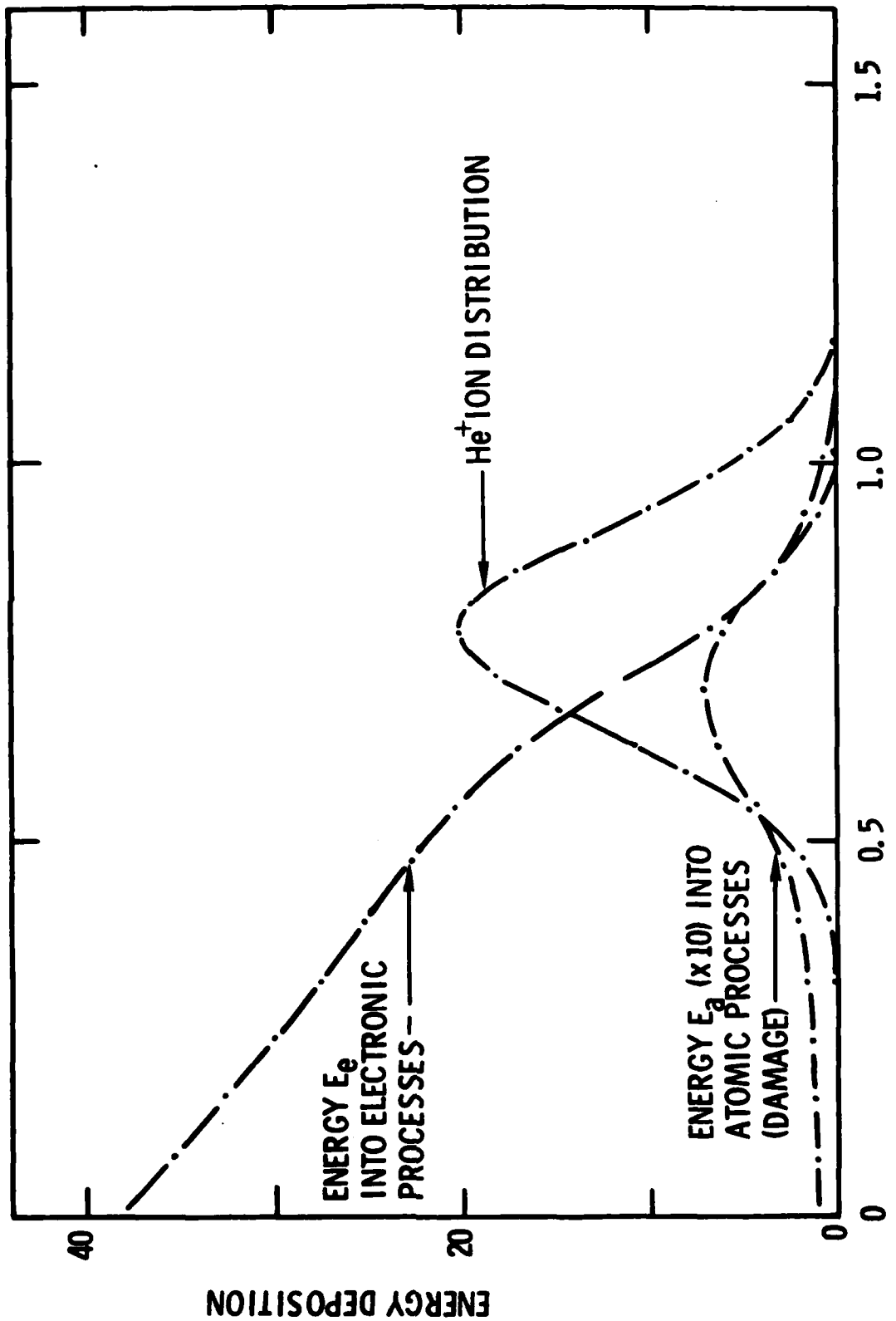
ENERGY DEPOSITION
40
20
0
0
0.5
1.0
1.5
DEPTH (μm)
He+ ION DISTRIBUTION
ENERGY Ee INTO ELECTRONIC PROCESSES
ENERGY Ea (x10) INTO ATOMIC PROCESSES (DAMAGE)

Figure 7

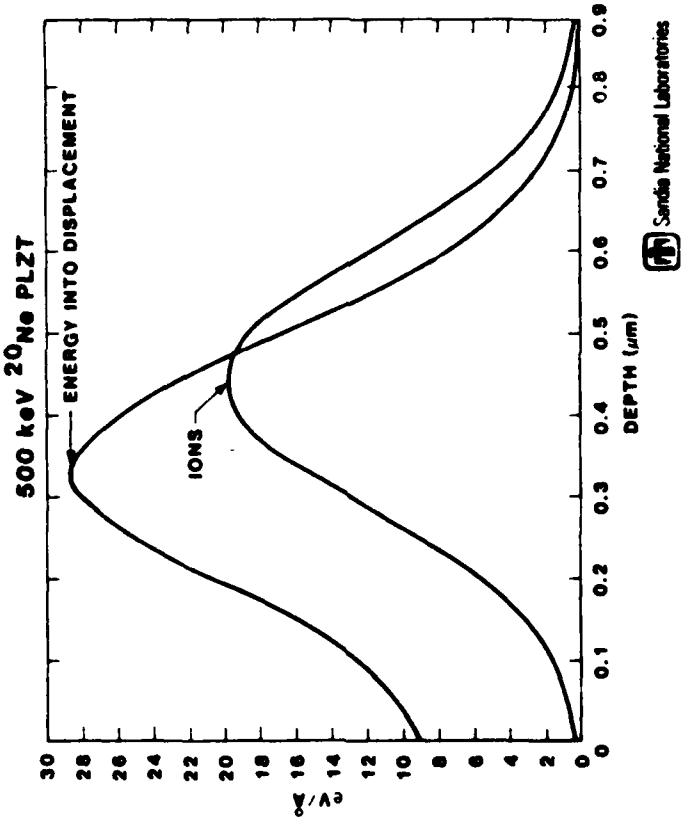
500 keV ^{20}Ne PLZT
ENERGY INTO DISPLACEMENT
IONS
eV/Å
DEPTH (μm)
Sandia National Laboratories

Figure 8

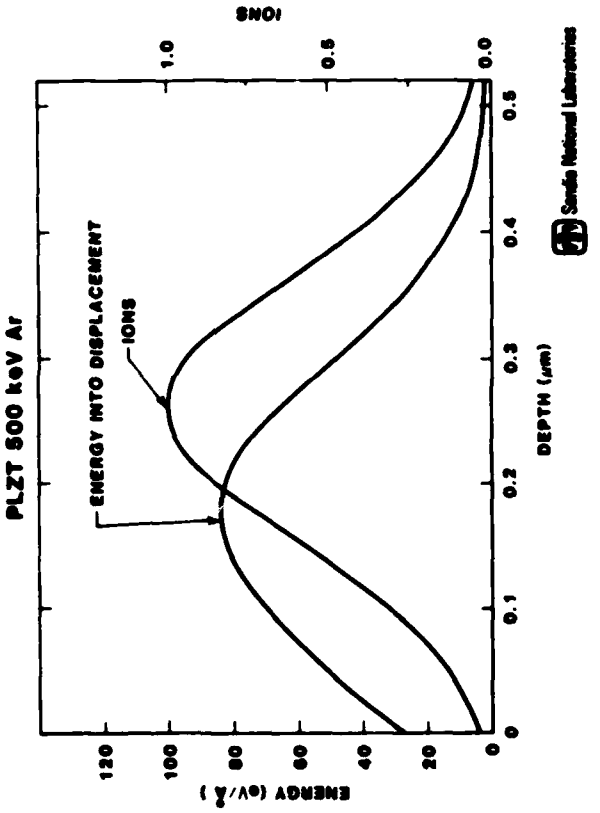
PLZT 500 keV Ar
ENERGY INTO DISPLACEMENT
IONS
ENERGY (eV/Å)
DEPTH (μm)
IONS
Sandia National Laboratories

Figure 9

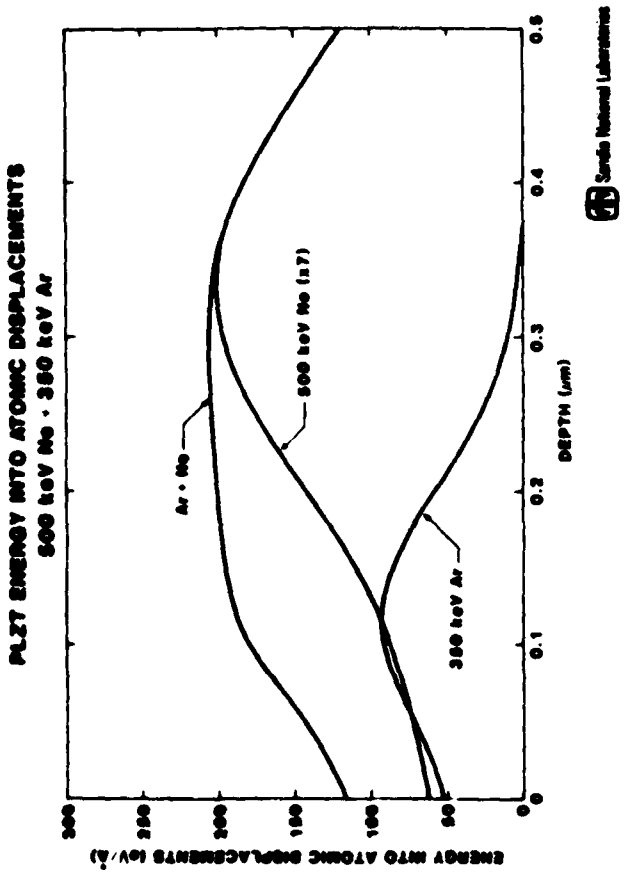
PLZT ENERGY INTO ATOMIC DISPLACEMENTS
500 keV Ne + 350 keV Ar
Ar + Ne
500 keV Ne (x7)
350 keV Ar
ENERGY INTO ATOMIC DISPLACEMENTS (eV/Å)
DEPTH (μm)
Sandia National Laboratories

Figure 10

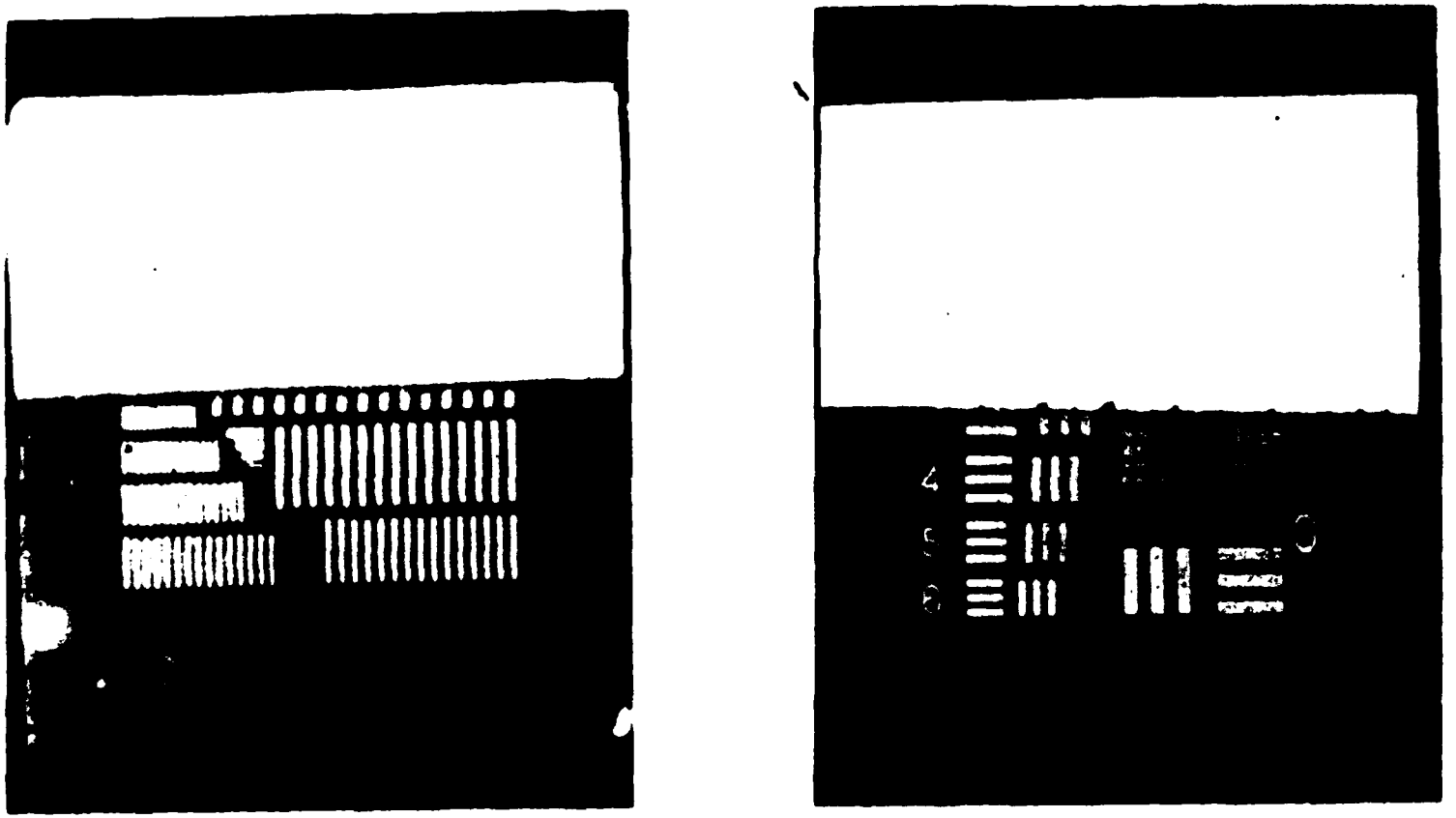

(A) (B)

Figure 11

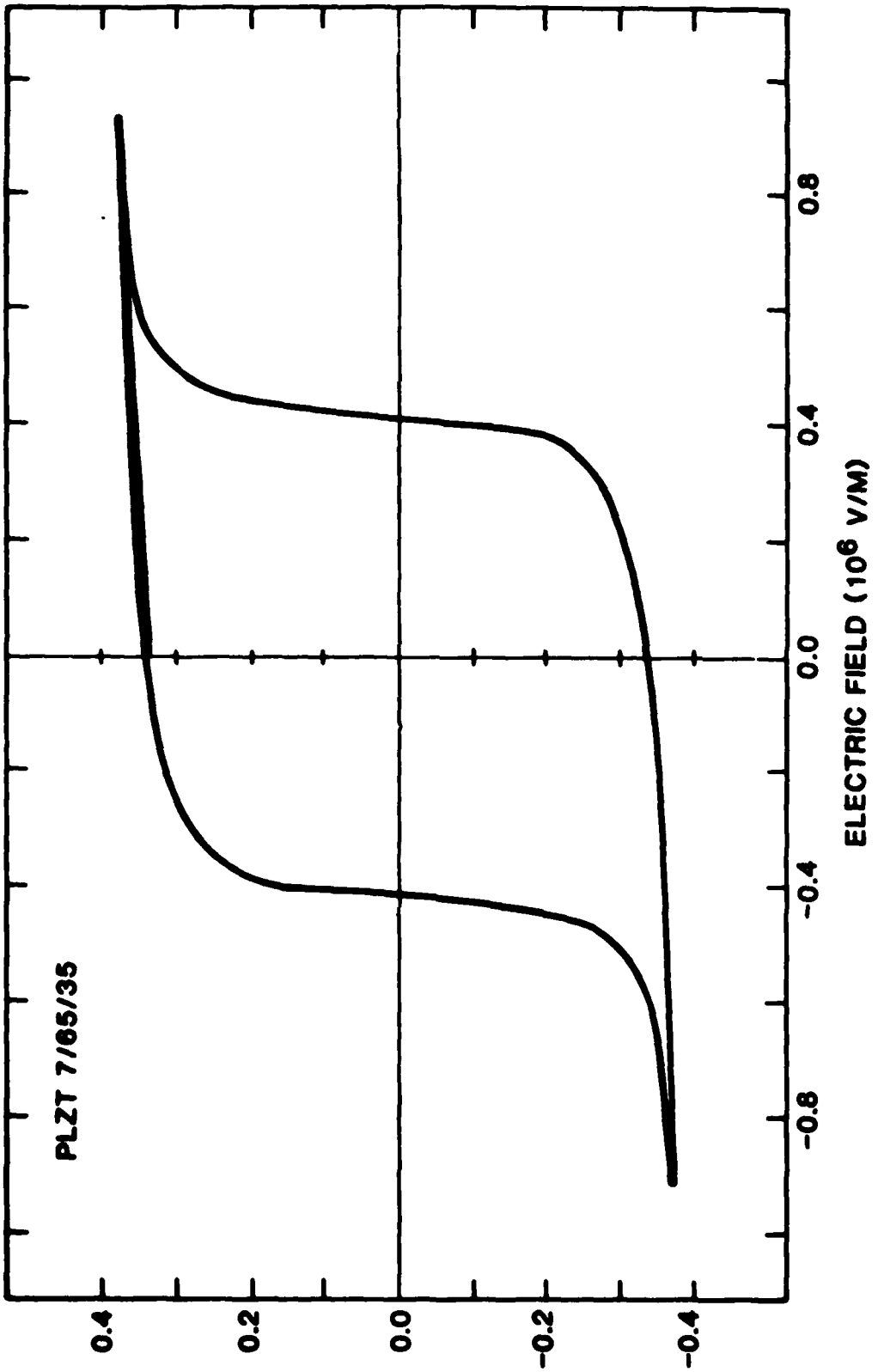
PLZT 7/65/35
ELECTRIC DISPLACEMENT (C/m²)
0.4
0.2
0.0
-0.2
-0.4
ELECTRIC FIELD (10⁶ V/M)
0.8
0.4
0.0
-0.4
-0.8

Figure 12

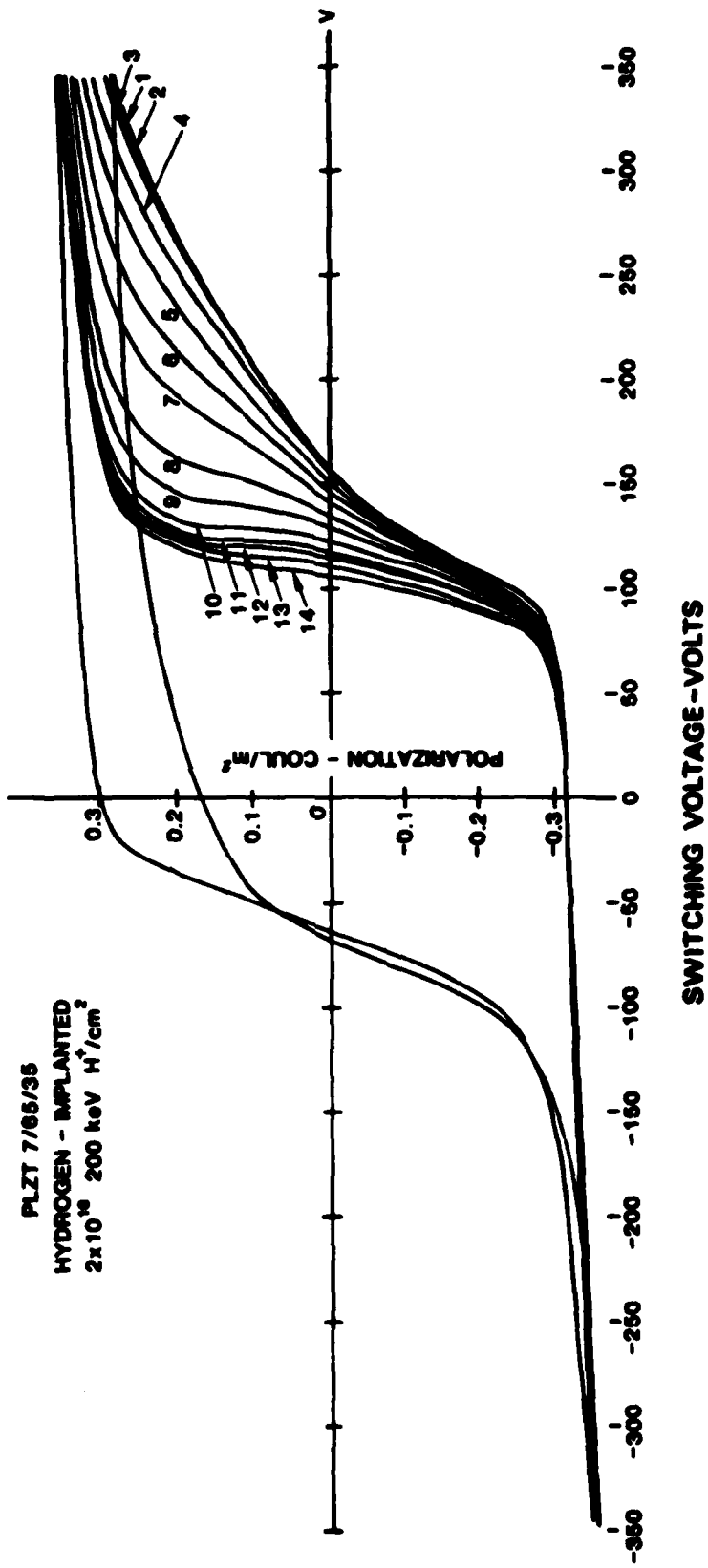
PLZT 7/65/35
HYDROGEN - IMPLANTED
2x10^15 200 keV H+/cm2
POLARIZATION - COUL/m2
SWITCHING VOLTAGE-VOLTS
V
0.3
0.2
0.1
0
-0.1
-0.2
-0.3
350
300
250
200
150
100
50
0
-50
-100
-150
-200
-250
-300
-350
1
2
3
4
5
6
7
8
9
10
11
12
13
14

Figure 13

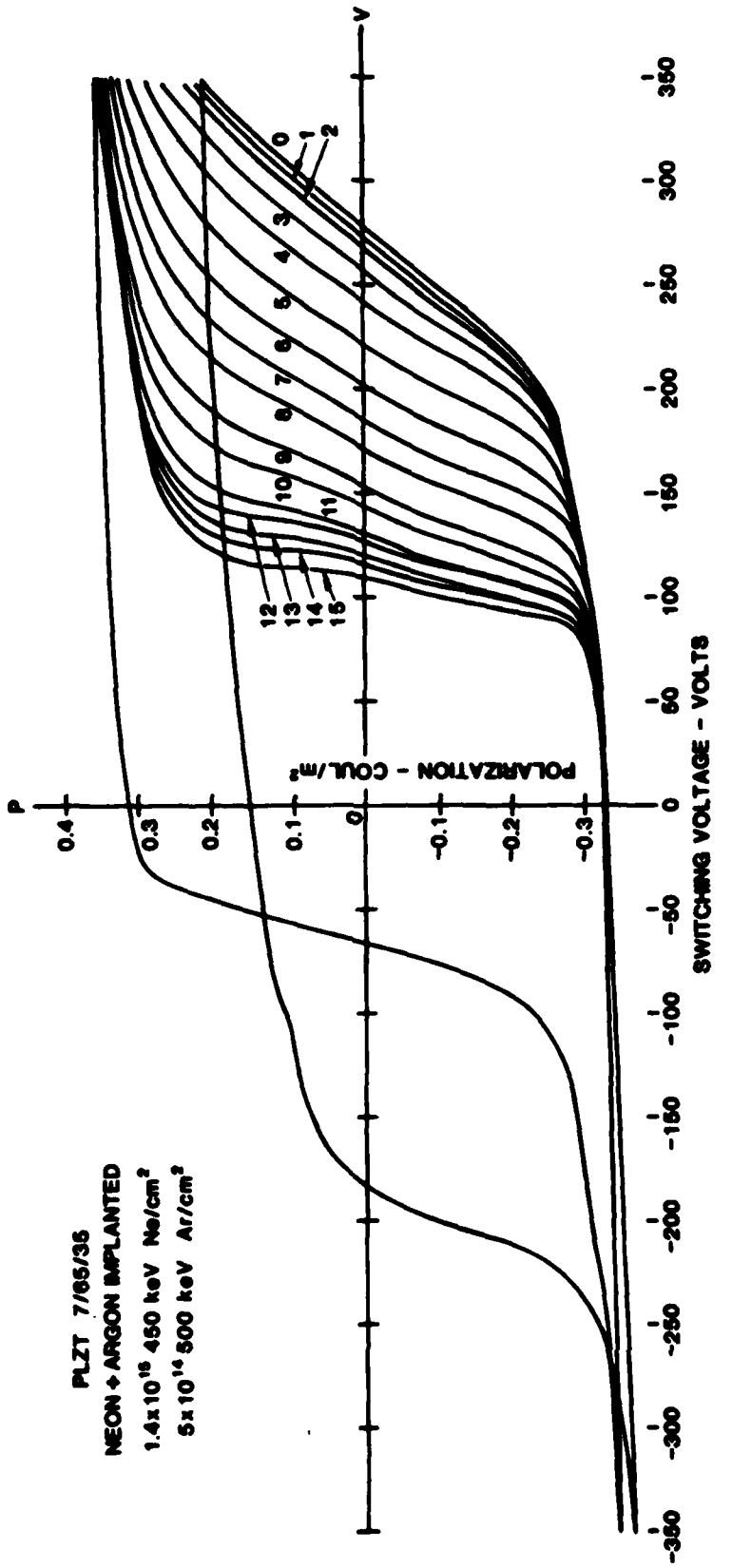
PLZT 7/65/35
NEON + ARGON IMPLANTED
1.4x10^15 450 keV Ne/cm^2
5x10^14 500 keV Ar/cm^2
P
V
POLARIZATION - COUL./m^2
SWITCHING VOLTAGE - VOLTS
0.4
0.3
0.2
0.1
0
-0.1
-0.2
-0.3
350
300
250
200
150
100
50
0
-50
-100
-150
-200
-250
-300
-350
0
1
2
3
4
5
6
7
8
9
10
11
12
13
14
15

Figure 14

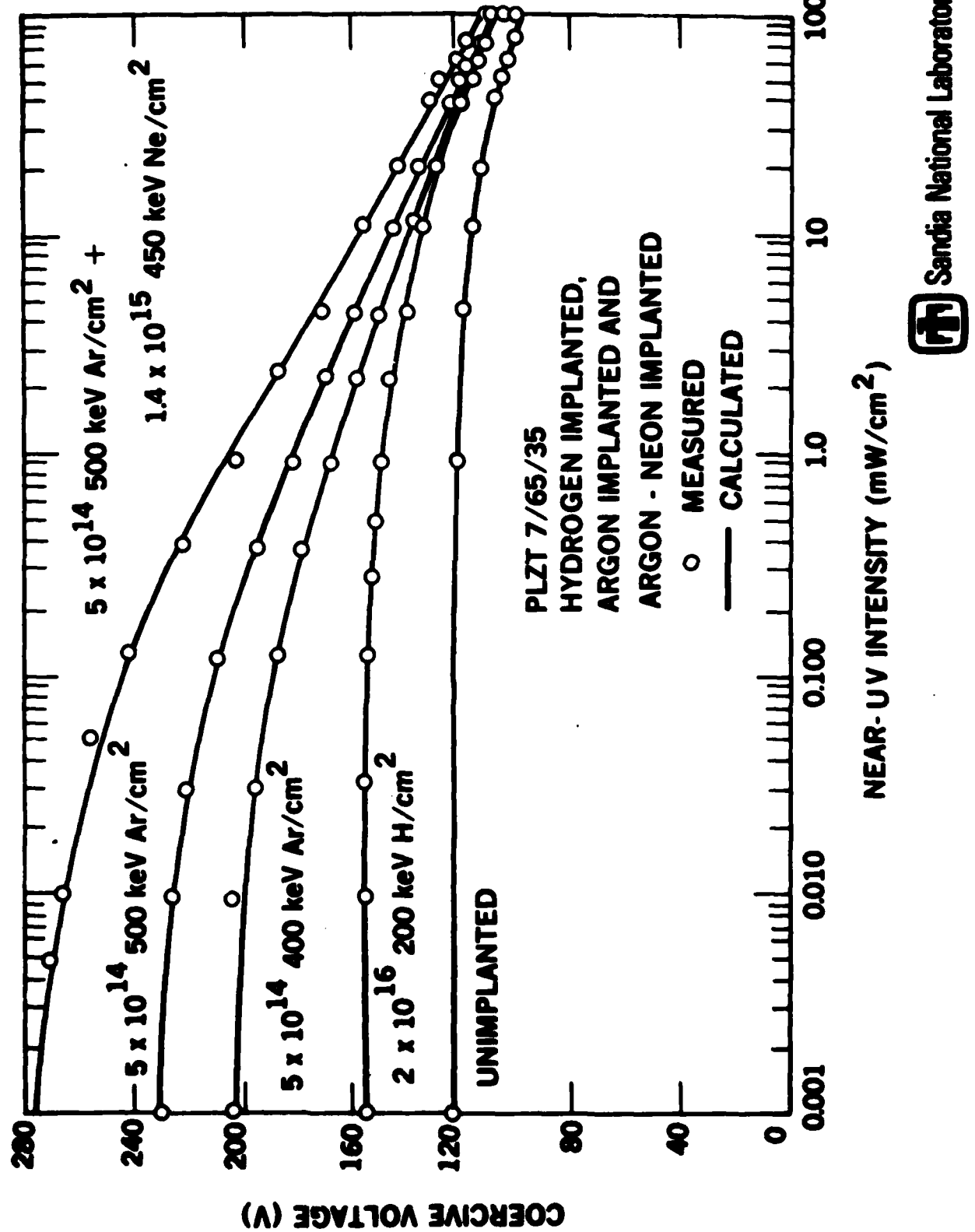
COERCIVE VOLTAGE (V)
280
240
200
160
120
80
40
0
0.001
0.010
0.100
1.0
10
100
NEAR-UV INTENSITY (mW/cm²)
Sandia National Laboratories
PLZT 7/65/35
HYDROGEN IMPLANTED,
ARGON IMPLANTED AND
ARGON - NEON IMPLANTED
o MEASURED
— CALCULATED
5 x 10¹⁴ 500 keV Ar/cm² + 1.4 x 10¹⁵ 450 keV Ne/cm²
5 x 10¹⁴ 500 keV Ar/cm²
5 x 10¹⁴ 400 keV Ar/cm²
2 x 10¹⁶ 200 keV H/cm²
UNIMPLANTED

Figure 15

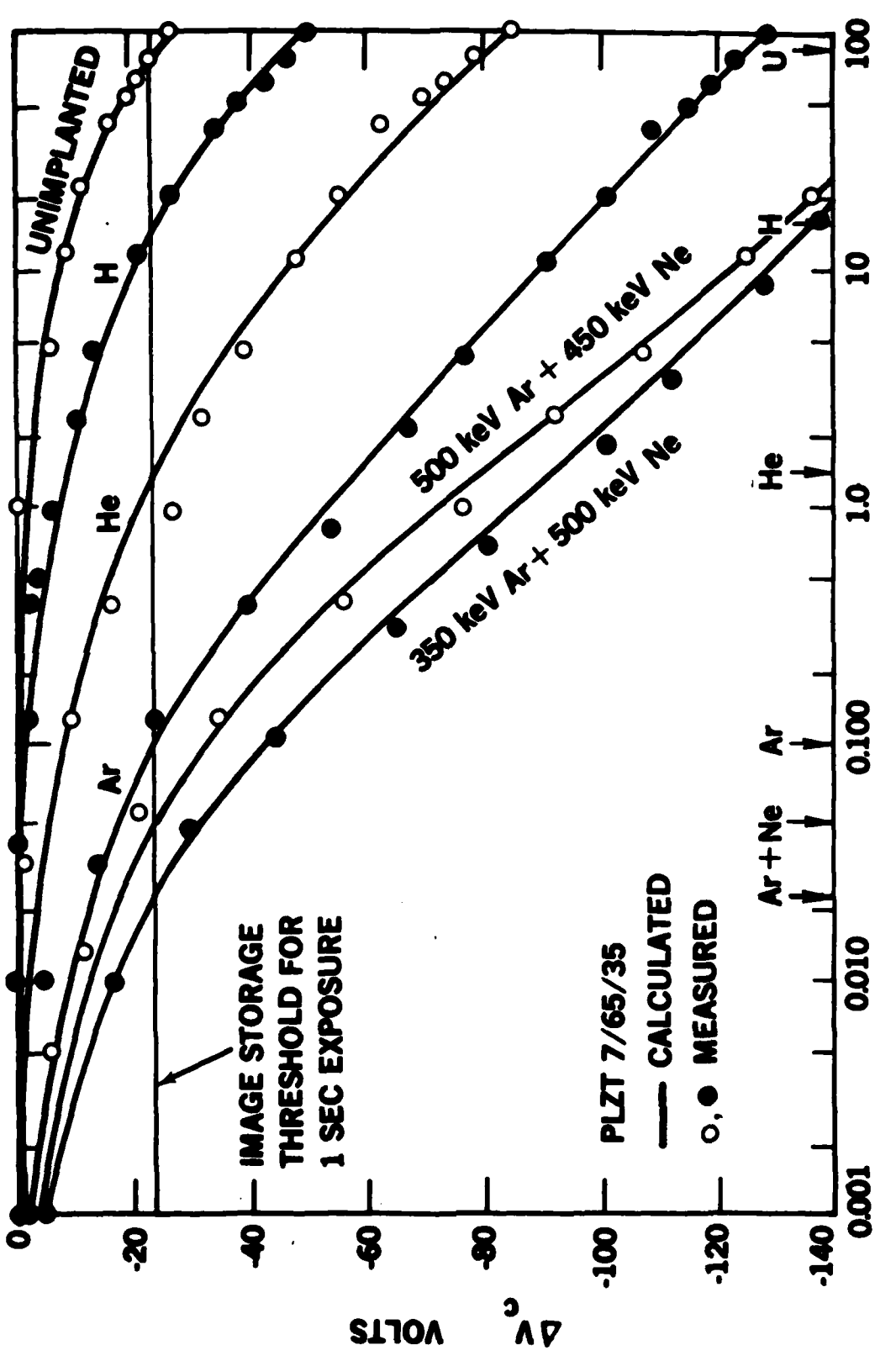
UNIMPLANTED
H
He
Ar
500 keV Ar + 450 keV Ne
350 keV Ar + 500 keV Ne
IMAGE STORAGE THRESHOLD FOR 1 SEC EXPOSURE
PLZT 7/65/35
— CALCULATED
○, ● MEASURED
Ar+Ne
Ar
He
H
U
0
-20
-40
-60
-80
-100
-120
-140
ΔV_c VOLTS
0.001
0.010
0.100
1.0
10
100
NEAR- UV INTENSITY (mW/cm²)
Sandia National Laboratories

Figure 16

PROPERTIES / PROCESSES	THRESHOLD SENSITIVITY E (ERGS/CM^2)	SPEED - ASA S = E^{-1} (ERGS/CM^2)$^{-1}$	SPECTRAL RANGE FOR STORAGE (NM)	SPECTRAL RANGE FOR READOUT (NM)	CONTRAST RANGE (OD)	SELECTIVELY ERASABLE	ELECTRICAL CONTRAST ENHANCEMENT	IMAGE VOLATILITY	MAXIMUM RESOLUTION (LINES/MM)	MAXIMUM IMAGE AREA (CM^2)	STORAGE VOLTAGE (VOLTS)
SILVER HALIDE FILM[1] (ASA-100)	10^{-2}	10^{2}	VIS.	VIS.	~3	NO	NO	NO	~200		
ELECTROPHOTOGRAPHY[1]	1	1	VIS.	VIS.	~2	NO	NO	NO	~100		
Bi_{12} Si O_{20} - PROM[2] IMAGE STORAGE	50 100 100	2×10^{-2} 10^{-2} 10^{-2}	436 405 492	633	~3	YES	YES	YES	~80	16	4000
PLZT CERAMICS AR + NE IMPLANTED	100	10^{-2}	365	VIS.	~2	YES	YES	NO	~40	175	400
Bi_{12} Si O_{20} - PROM PHOTOREFRACTIVE[3]	3×10^{3}	3×10^{-4}	442	633		NO	NO	YES	~100	16	4000
PLZT CERAMICS UNIMPLANTED	10^{6}	10^{-6}	365	VIS.	~2	YES	YES	NO	~40	175	400
DIAZO[1]	10^{6}	10^{-6}	VIS.	VIS.	~1	NO	NO	NO			

(1) J. C. DAINTY & R. SHAW, IMAGE SCIENCE, ACADEMIC PRESS, LONDON (1974), PP. 48-49

(2) S. G. LIPSON & P. NISENSON, APPLIED OPTICS 13, PP. 2052-2060 (SEPT. 1974)

(3) F. MICHERON, FERROELECTRICS 18, PP. 153-159 (1978)

Table I

Publications Resulting from Reported Work

1. C. E. Land and P. S. Peercy, "New Image Storage Mechanisms in PLZT Ceramics Using Near-Ultraviolet Light," 1976 IEEE-SID Biennial Display Conf. Record, pp. 71-75, Oct. 1976.

2. C. E. Land and P. S. Peercy, "Photoferroelectric Image Storage in PLZT Ceramics," Info. Display J. 13, pp. 20-26, 1977.

3. C. E. Land, "Information Storage and Display Techniques Using PLZT Ceramics," Proc. Soc. of Photo-Optical Inst. Engr. 83, pp. 44-50, Aug. 1976.

4. C. E. Land and P. S. Peercy, "Photoferroelectric Effects in PLZT Ceramics," Ferroelectrics 22, pp. 677-679, 1978.

5. C. E. Land, "Optical Information Storage and Spatial Light Modulation in PLZT Ceramics," Optical Engrg 17, pp. 317-326, 1978.

6. C. E. Land and P. S. Peercy, "Photoferroelectric Image Storage and Contrast Modification in PLZT Ceramics," Soc. for Info. Display Intl. Symp. Digest of Tech. Papers 9, pp. 14-15, April 1978.

7. C. E. Land, "Photoferroelectric Image Storage in Antiferroelectric Phase PLZT Ceramics," 1978 IEEE-SID Biennial Display Research Conf. Record, pp. 38-41, Oct. 1978; IEEE Trans. on Electron Dev. ED-26, pp. 1143-1147, Aug. 1979; Proc. Soc. for Info. Display 20, pp. 219-223, 1979.

8. C. E. Land and P. S. Peercy, "Ion-Implanted PLZT for Photoferroelectric Image Storage and Display Device," Ferroelectrics 27, pp. 131-136, 1980.

9. C. E. Land and P. S. Peercy, "Enhanced Sensitivity of Photoferroelectric Image Storage in Ion-Implanted PLZT Ceramics," Soc. for Info. Display Intl. Symp. Digest of Tech. Papers 11, pp. 220-221, April 1980.

10. C. E. Land and P. S. Peercy, "Photosensitivity Enhancement by H- and He-Ion Implantation in Lead Lanthanum Zirconate Titanate Ceramics," Appl. Phys. Lett. 37., pp. 39-41, July 1980.

11. P. S. Peercy and C. E. Land, "Optical Image Storage in Ion-Implanted PLZT Ceramics," Proc. Ion Beam Mod. of Matls. Conf., July 1980.

12. C. E. Land, "Effects of Photoferroelectric Space Charge Fields on Visible-Light Scattering in PLZT Ceramics," Ferroelectrics 27, pp. 143-146, 1980.

13. Peter J. Chen and C. E. Land, "Variations of Strain and Light Scattering Accompanying Domain Switching in Lead Lanthanum Zirconate Titanate Ceramics," J. Appl. Phys. 51, pp. 4961-4966, Sept. 1980.

14. P. S. Peercy and C. E. Land, "A Model for Ion-Implantation-Induced Improvements of Photoferroelectric Imaging in Lead Lanthanum Zirconate Titanate Ceramics," Appl. Phys. Lett. 37, pp. 815-818, Nov. 1980.

15. P. S. Peercy and C. E. Land, "Ion-Implanted PLZT Ceramics: A New High-Sensitivity Image Storage Medium," 1980 IEEE-SID Biennial Display Research Conf. Record, pp. 133-139, Oct. 1980; also, to be published in IEEE Trans. on Electron Devices ED-28, 1981, and Proc. Soc. for Info. Display 22, 1981.

16. P. S. Peercy and C. E. Land, "PLZT Photoferroelectric Sensitivity Enhancement by Ion-Implantation," Am. Cer. Soc. Bull. 59, (Abstract) p. 829, Aug. 1980.

17. C. E. Land, "Photoferroelectric Imaging," McGraw-Hill Encyclopedia of Science and Technology, 5th Edition, McGraw-Hill, New York (1981).

18. P. S. Peercy and C. E. Land, "Photosensitivity Enhancement of PLZT Ceramics by Positive Ion Implantation," U. S. Patent Application, Case S-50,942, Filed 1980.

Scientific Personnel Participating in this Project

1. Principal Investigator

   Cecil E. Land, Member of Technical Staff, Solid State Device Physics Division

2. Co-investigator

   Paul S. Peercy, Supervisor of Technical Staff, Ion Implantation Physics Division

3. Staff Associate

   Ira D. McKinney, Technical Staff Associate, Solid State Device Physics Division

4. Consultant

   George A. Samara, Department Manager, Condensed Matter and Device Physics Research Department

SECURITY CLASSIFICATION OF THIS PAGE (When Data Entered)

REPORT DOCUMENTATION PAGE	READ INSTRUCTIONS BEFORE COMPLETING FORM
1. REPORT NUMBER	2. GOVT ACCESSION NO. AD-A097 448	3. RECIPIENT'S CATALOG NUMBER
4. TITLE (and Subtitle) Photoferroelectric Image Storage in PLZT Ceramics	5. TYPE OF REPORT & PERIOD COVERED Final Report February 1978 to February 1981
	6. PERFORMING ORG. REPORT NUMBER
7. AUTHOR(s) Cecil E. Land and Paul S. Peercy	8. CONTRACT OR GRANT NUMBER(s) 1L161102BH57-07 Physics AT(29-1)-789
9. PERFORMING ORGANIZATION NAME AND ADDRESS Sandia National Laboratories P. O. Box 5800 Albuquerque, NM 87185	10. PROGRAM ELEMENT, PROJECT, TASK AREA & WORK UNIT NUMBERS
11. CONTROLLING OFFICE NAME AND ADDRESS U. S. Army Research Office P. O. Box 12211 Research Triangle Park, NC 27709	12. REPORT DATE March 1981
	13. NUMBER OF PAGES 49
14. MONITORING AGENCY NAME & ADDRESS(if different from Controlling Office)	15. SECURITY CLASS. (of this report) Unclassified
	15a. DECLASSIFICATION/DOWNGRADING SCHEDULE

16. DISTRIBUTION STATEMENT (of this Report)

Approved for public release; distribution unlimited.

17. DISTRIBUTION STATEMENT (of the abstract entered in Block 20, if different from Report)

N/A

18. SUPPLEMENTARY NOTES

The findings in this report are not to be construed as an official Department of the Army position, unless so designated by other authorized documents.

19. KEY WORDS (Continue on reverse side if necessary and identify by block number)

photographic imaging	erasable image store
photoferroelectric effects	image contrast enhancement
ferroelectric ceramics	photosensitivity enhancement
ion implantation in ferroelectrics	holographic storage medium

20. ABSTRACT (Continue on reverse side if necessary and identify by block number)

The photosensitivity of lead lanthanum zirconate titanate (PLZT) ceramics is increased by as much as four orders of magnitude by implantation of inert gas ions in the image storage surface. The photoferroelectric image storage device can be used as a temporary image store, for contrast enhancement of the stored image, and for holographic storage.

DD FORM 1 JAN 73 1473 EDITION OF 1 NOV 65 IS OBSOLETE unclassified


DAT
ILM